JGR Atmospheres

RESEARCH ARTICLE
10.1029/2019JD031503

A Damping Effect of the Maritime Continent for the Madden-Julian Oscillation

Xianan Jiang[1,2], Hui Su[2], and Duane E. Waliser[2]

[1]Joint Institute for Regional Earth System Science & Engineering, University of California, Los Angeles, CA, USA, [2]Jet Propulsion Laboratory, California Institute of Technology, Pasadena, CA, USA

Key Points:
- The MJO damping over the MC is linked to a drying effect due to advection of the topographically locked mean moisture by MJO winds
- The diurnal cycle plays a crucial role for the formation of the topographically locked mean moisture pattern over the MC
- High-resolution models capable of resolving MC topography and diurnal cycle will be needed to represent interaction between the MC and MJO

Correspondence to:
X. Jiang,
xianan@ucla.edu

Citation:
Jiang, X., Su, H., & Waliser, D. E. (2019). A damping effect of the maritime continent for the madden-julian oscillation. *Journal of Geophysical Research: Atmospheres*, *124*, 13,693–13,713. https://doi.org/10.1029/2019JD031503

Received 13 AUG 2019
Accepted 20 NOV 2019
Accepted article online 25 NOV 2019
Published online 21 DEC 2019

Author Contributions:
Conceptualization: Xianan Jiang
Formal analysis: Xianan Jiang
Funding acquisition: Xianan Jiang
Investigation: Xianan Jiang, Hui Su, Duane E. Waliser
Writing - original draft: Xianan Jiang, Hui Su, Duane E. Waliser
Writing – review & editing: Xianan Jiang, Hui Su, Duane E. Waliser

Abstract The damping effect of the Maritime Continent (MC) on propagation of the Madden-Julian Oscillation (MJO) has been widely recognized; however, its underlying physics remains largely elusive. Capitalizing on the latest high-resolution reanalysis data (ERA-5) from the ECMWF, analyses in this study suggest that the interruption of lower-tropospheric moistening over the MC land during MJO eastward propagation is mainly due to a drying effect induced by zonal advection of the low-level winter mean moisture by MJO winds. The low-level mean moisture pattern over the MC tends to closely follow local topography, with moisture maxima collocated with local mountain peaks. Given this mean moisture distribution, the moisture advection by anomalous easterly MJO winds corresponding to the active MJO convection over the eastern Indian Ocean will lead to a drying (moistening) effect to the east (west) of the mountain peaks. Diagnosis based on hourly output from ERA-5 further illustrates that the diurnal cycle plays a crucial role for the formation of the topographically locked mean moisture pattern over the MC. This study, therefore, indicates that high-resolution models capable of resolving detailed topography and associated diurnal cycle over the MC could be necessary for realistic depiction of the interaction between the MC and MJO.

1. Introduction

The important role of the Madden-Julian Oscillation (MJO; Madden & Julian, 1971) in the global hydrological cycle has been widely recognized (Lau & Waliser, 2012; Zhang, 2005), not only due to its tremendous influences on climate and weather extremes worldwide (e.g., Zhang, 2013) but also its critical role for short-term climate prediction (Vitart et al., 2012). The MJO, however, still remains poorly represented even in the latest global climate and weather forecast models (e.g., Ahn et al., 2017; Jiang et al., 2015; Kim et al., 2014; Lim et al., 2018; Neena et al., 2014; Vitart, 2017; Xiang et al., 2015). One of the grand challenges in modeling and predicting the MJO lies in its interaction with multi-scale convective elements (e.g., Chen et al., 1996; Kiladis et al., 2009; Mapes et al., 2006; Moncrieff, 2013; Nakazawa, 1988; Takayabu, 1994), particularly when complex topography is involved, for example, over the Maritime Continent (MC) region.

Situated in the heart of the Indo-Pacific warm pool, the MC is characterized by heavy annual rainfall, which plays a crucial role in driving the global atmospheric circulation through latent heat release (Neale & Slingo, 2003; Ramage, 1968; Slingo et al., 2003). Due to land-ocean contrast and local high mountains (Figure 1), a large portion of the total annual rainfall over the MC occurs via a vigorous diurnal cycle (e.g., Kikuchi & Wang, 2008; Mori et al., 2004; Nesbitt & Zipser, 2003; Peatman et al., 2014; Qian, 2008; Yang & Slingo, 2001b). A number of studies have shown that the MC often acts as a "barrier" for the eastward propagation of the MJO (e.g., Kerns & Chen, 2016; Kim et al., 2014; Salby & Hendon, 1994; Seo & Kim, 2003), with the underlying physics being poorly understood and represented in high-resolution models or even the cloud-system resolving models (CRM; e.g., Love et al., 2011; Peatman et al., 2015; Birch et al., 2016; Hagos et al., 2016). These model shortcomings lead to limited skill in predicting the MJO when crossing the MC, a predicament often referred as the "MC prediction barrier" for the MJO (e.g., Vintzileos & Pan, 2008; Vitart & Molteni, 2010; Weaver et al., 2011; Fu et al., 2013; Wang et al., 2013; *Kim et al.*, 2014b; Kim et al., 2018).

Several factors have been proposed to be, at least partly, responsible for damped MJO amplitude over the MC, including a blocking effect from the MC topography (Hsu & Lee, 2005; Inness & Slingo, 2006; Wu & Hsu, 2009), and a lack of moist energy supply via surface fluxes over the MC land (Kim et al., 2011; Maloney & Sobel, 2004; Sobel et al., 2008). In addition, the vigorous local diurnal cycle is also considered

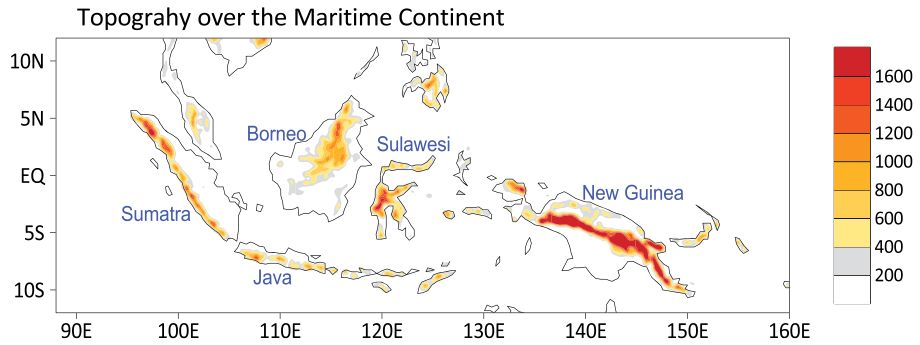

Figure 1. Elevation of topography over the Maritime Continent (unit: m).

to play a role in damping the MJO when propagating over the MC by limiting the available moist energy (e.g., Neale & Slingo, 2003; Zhang & Hendon, 1997). It was also suggested that whether or not the MJO can pass through the MC is subject to a competition between local land and oceanic convection and that the development of oceanic convection over the MC region is critical to promote MJO propagation over the MC (Ling et al., 2019; Zhang & Ling, 2017). In a recent idealized modeling study, Majda and Yang (2016) proposed that upscale heat transport by the diurnal circulation can effectively suppress MJO deep convection when it propagates into the MC. Based on CRM simulations, Hagos et al. (2016) demonstrated that the eastward propagation of an MJO event over the MC can be significantly enhanced after switching off the diurnal cycle in the model, while the model MJO is quickly damped over the MC if the diurnal effect is present.

Strong modulation of the diurnal cycle of precipitation over the MC by the MJO indeed has been widely reported (e.g., Love et al., 2011; Oh et al., 2012; Peatman et al., 2014; Rauniyar & Walsh, 2011; Tian et al., 2006). Based on the International Satellite Cloud Climatology Project (ISCCP) cloud product, Tian et al. (2006) suggested that the diurnal cycle of tropical deep convective clouds over the MC is enhanced (reduced) over both land and ocean during active (break) phase of the MJO, with no significant modulation of the diurnal phase by the MJO. By analyzing TRMM precipitation observations, Rauniyar and Walsh (2011) found that the strongest diurnal cycle of precipitation over the MC land occurs during the suppressed phase of the MJO, defined by the MJO phases 7–8 and 1–3 based on the Wheeler-Hendon MJO index (Wheeler & Hendon, 2004), while strongest rainfall diurnal cycle over the MC ocean during the convectively active MJO phases 4–6. Oh et al. (2012) and Peatman et al. (2014) also illustrated enhanced diurnal cycle of rainfall over the MC land (~15%–25% over the climate) during the MJO phase 3, suggesting a vanguard of precipitation over the MC islands 1 week prior to the arrival of the peak MJO convection when convection over the surrounding MC seas is still suppressed (Peatman et al., 2014). Oh et al. (2012) also suggested that precipitation is more intense over the Java Sea in the morning during the mature MJO phase over the MC. Representation of these observed diurnal cycle of precipitation over the MC and its modulation by the MJO, however, is greatly challenging in global climate models (GCMs; e.g., Yang & Slingo, 2001b; Love et al., 2011; Peatman et al., 2015; Baranowski et al., 2019).

Despite these above-mentioned hypotheses, the underlying physical processes for the damping effect of the MC on MJO eastward propagation largely remain elusive. In this study, we capitalize on the recently released high-resolution ERA-5 reanalysis to examine the interactions between the MC and MJO. Specifically, we focus our analyses on the interruption of moisture preconditioning over the MC during the MJO propagation from the Indian Ocean (IO) to the western Pacific, to characterize the underlying processes associated with the MC damping effect on the MJO. The outline of this paper is as follows. In Section 2, the observational dataset used for this study is introduced. The damping effect of the MC on the MJO is illustrated in Section 3. Modulation of the MC diurnal cycle by the MJO is examined in Section 4. In Section 5, key processes responsible for the MC damping effect for the MJO are explored by analyzing moisture tendency terms over the MC region associated with enhanced MJO convection over the eastern IO (EIO). A summary and discussions are presented in Section 6.

2. Observational Datasets

The primary observational dataset used for this study is the latest high-resolution ERA-5 reanalysis from the ECMWF with a horizontal resolution of approximately 30 km at hourly time intervals (ECMWF, 2017). ERA-5 was produced using 4D-Var data assimilation in CY41R2 of the ECMWF's Integrated Forecast System (IFS), with 137 hybrid sigma/pressure model levels in the vertical and the top level at 0.01 hPa. Improvements to ERA-5, compared to its earlier generation, that is, the ERA-Interim reanalysis (Dee et al., 2011), include the use of the Met-Office Hadley Centre's sea ice and sea surface temperature dataset version 2 (HadISST.2), reprocessed ECMWF climate data records, and implementation of an updated radiative transfer model for the TIROS Operational Vertical Sounder. Variational bias corrections have not only been applied to satellite radiances, but also ozone retrievals, aircraft observations, surface pressure, and radiosonde profiles. Variables analyzed in this study include interpolated 3D variables (winds, vertical velocity, moisture, temperature) at 37 pressures and 2D variables (precipitation, 2m temperature, and the convective available potential energy).

TRMM-based precipitation observations (version 3B42 v7; Huffman et al., 1995; TRMM, 2011) are also used to provide verification for the ERA-5 reanalysis. TRMM 3B42 is a global precipitation product based on multi-satellite and rain gauge analysis. It provides precipitation estimates with 3-hourly temporal resolution on a 0.25° spatial resolution in a global belt between 50°S and 50°N. Since only the ERA-5 data from 2010 to 2016 were available at the time of this study, both reanalysis and TRMM data during this period are employed in this study. Also, we limit our analysis for the extended boreal winter season from November to March due to the prevalence of the MJO eastward propagation over the MC during this period.

3. Damping Effect of the MC on the MJO

Figure 2a illustrates evolution of MJO precipitation when it passes over the MC region based on TRMM observations, derived by lag-regressed patterns of 20–80 day bandpass filtered precipitation against its averaged value over an EIO box (85–95°E; 5°S to 5°N). Before conducting regressions, the precipitation field is subject to removal of the climatological annual cycle (annual mean plus three leading annual harmonics) and then a 20–80 day filtering by applying a Lanczos bandpass time filter (Duchon, 1979). The statistical significance of the regression coefficients is assessed by testing the null hypothesis that the corresponding correlation coefficients are different from zero, through application of a two-sided Student's t test. Due to the time filtering, the number of degrees of freedom (DOF) is greatly reduced as compared to the original sample size (about 960 daily values). The effective DOF for rainfall at each grid point over the tropical Indo-Pacific region is estimated based on the lag-one auto-correlation following Bretherton et al. (1999) and is found to be about 40.

At lag day −3, when the MJO convection center is located over the EIO near 87°E, enhanced precipitation starts to emerge over the western part of Borneo while convection over the neighboring waters of the MC is still suppressed, reminiscent of the rainfall "vanguard" over the MC prior to the MJO convection as previously reported (Peatman et al., 2014). In the following days, the main MJO convection starts to cross over the MC. The largely suppressed precipitation over the MC region at day −3 is gradually replaced by enhanced precipitation anomalies after day 0. At day 6, the main MJO precipitation is largely scattered over the oceanic regions of the MC, with its amplitude significantly weakened from its earlier stage over the EIO. The particularly weak MJO convection over the MC islands as readily seen at day 6, clearly indicating the damping effects of the MC islands for the MJO. The oceanic pathway during the MJO propagation over the MC has also been previously discussed (e.g., Kim et al., 2017; Oh et al., 2012; Zhang & Ling, 2017).

The observed propagation characteristics of the MJO during its passage over the MC is well represented in the ERA-5 reanalysis (Figure 2b) although the amplitude of MJO precipitation in the reanalysis is generally weaker than that in the TRMM observations, which was also found with the ERA-Interim reanalysis (e.g., Adames, 2017). The weakened MJO convective signals over the MC, particularly over the land region, relative to the EIO as seen in TRMM is well captured in the ERA-5 reanalysis (e.g., day 6). Therefore, in-depth diagnosis using ERA-5 output provides a great opportunity to understand the essential processes responsible for the damping effect of the MC islands on MJO convection. In particular, the hourly interval of the ERA-5 data makes it possible to explore interaction between the local diurnal cycle and the MJO.

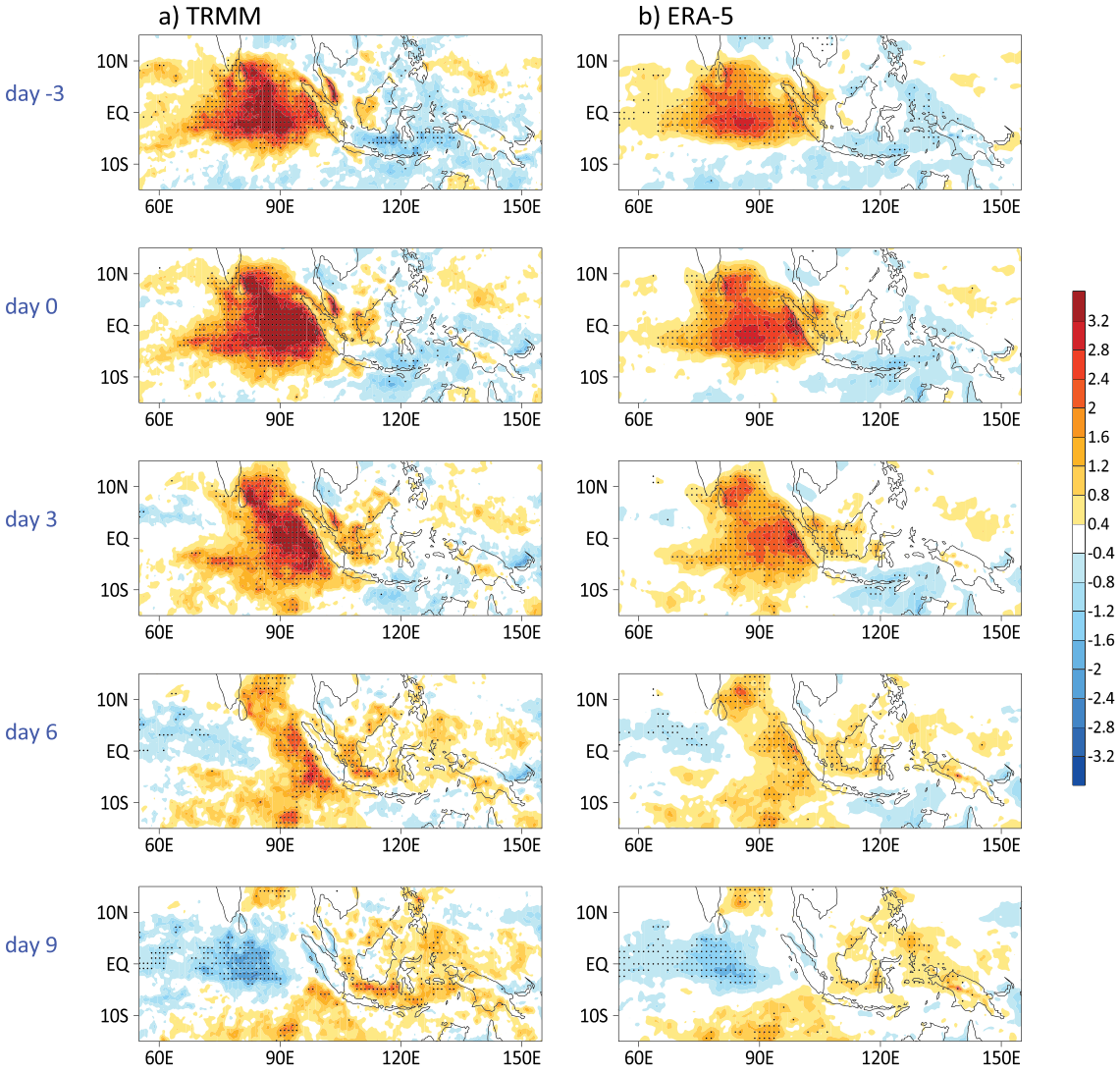

Figure 2. Evolution of MJO precipitation anomalies (unit: mm day^{-1}) as denoted by lag-regression of 20–80 day bandpass filtered precipitation against its averaged value in an EIO box (85–95°E; 5°S to 5°N) based on TRMM observations (left) and the ERA-5 reanalysis (right) for winters (Nov-Mar) from 2010 to 2016. Grids where rainfall anomalies are significant at 95% level are stippled based on the Student's *t* test of corresponding lag-correlation coefficients.

4. Modulation of the Diurnal Cycle Over the MC by the MJO Over the EIO

The upscale impact by diurnal convection has been proposed to play an important role in weakening the MJO when propagating into the MC (e.g., Hagos et al., 2016; Majda & Yang, 2016), which is supported by modulations of the MC diurnal cycle by the MJO (e.g., Oh et al., 2012; Peatman et al., 2014). In this part, we examine how the MC diurnal cycle is modulated by the MJO with a focus over the west MC islands, including Sumatra and Borneo, when the MJO convection is located right to the west of the MC (e.g., between day −3 and day 0 in Figure 2). This will provide insights into the potential role of the diurnal cycle in generating upscale tendencies on MJO moisture, heat, and momentum, thus affecting MJO amplitude when it further propagates eastward. For this purpose, Figures 3 and 4 illustrate 3-hourly precipitation evolution during enhanced and suppressed phases of MJO convection over the EIO based on both TRMM and ERA-5. Enhanced (suppressed) MJO periods are selected by the days corresponding to positive (negative) peaks of 20–80 day filtered precipitation averaged over the 80–90°E, 5°S to 5°N that exceed one standard deviation, as well as the following 4 days after the peak days. Anomalous rainfall pattern during the enhanced MJO phase largely resembles that between day −3 and day 0 as shown in Figure 2 and with an

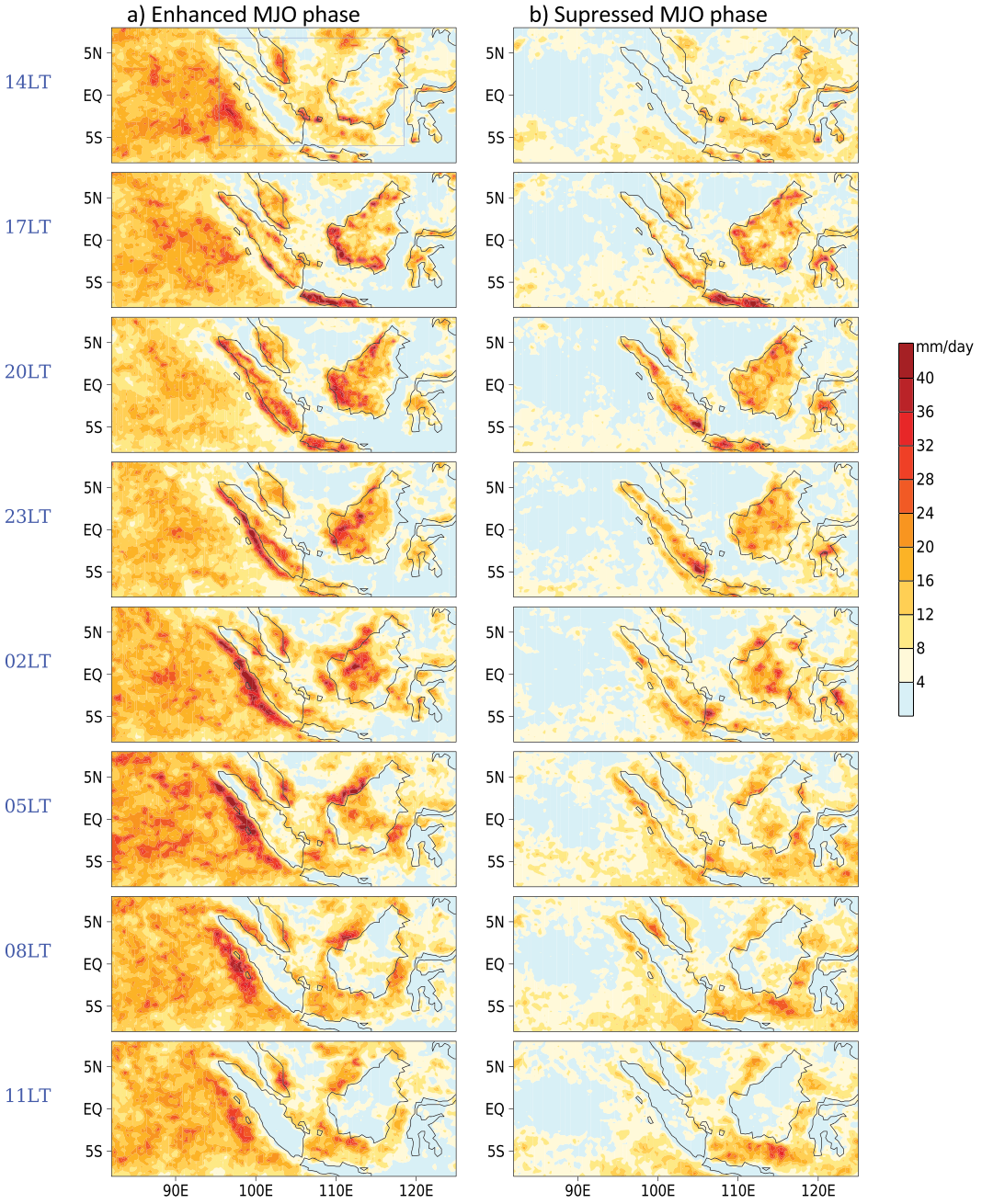

Figure 3. Composite diurnal precipitation (unit: mm day^{-1}) evolution based on TRMM observations for convectively enhanced (left) and suppressed (right) periods of the MJO over the EIO. See text for detailed definition of the enhanced and suppressed MJO periods.

opposite sign for the suppressed MJO phase. By this approach, 105 and 95 days are identified as enhanced and suppressed MJO days during the seven winters, respectively. Composites of diurnal precipitation evolution for the two MJO periods can then be derived.

Figure 3 shows that during the enhanced MJO period (left panels), persistent precipitation is observed over the EIO throughout the day, with the heaviest precipitation in the local early morning, in agreement with many previous studies on the diurnal cycle over tropical oceans (e.g., Yang & Slingo, 2001b). Note that the local time over the MC here is defined by the Singapore Standard Time, which is 8 hr ahead of Coordinated Universal Time (UTC). Over the MC land, precipitation starts to form over the coastal region

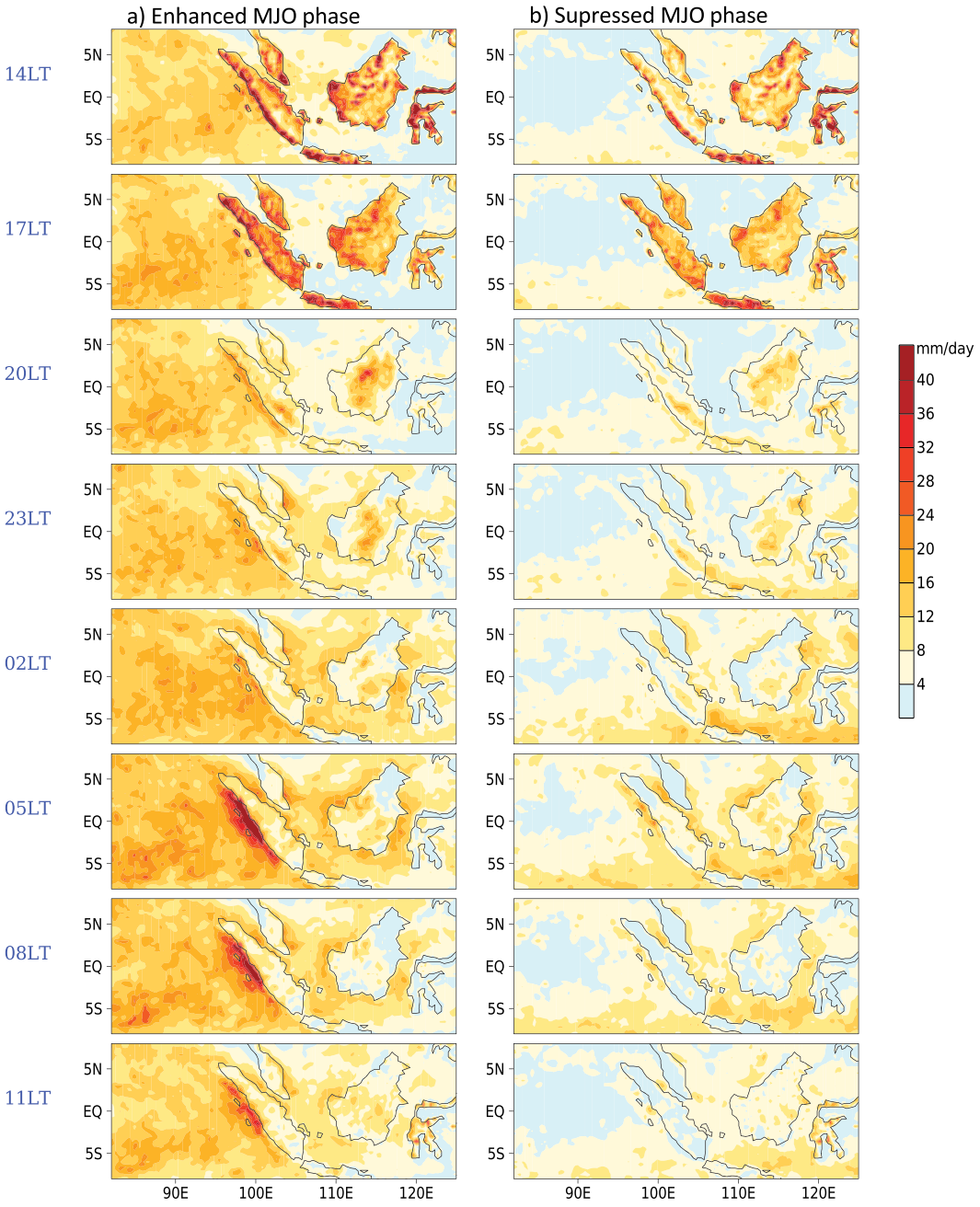

Figure 4. Same as in Figure 3, but based on the ERA-5 reanalysis.

after 14LT on both Sumatra and Borneo and then moves inland. Precipitation over the land reaches its maximum near 20LT and subsequently retreats back towards the coast. In particular, a well-organized southeast-northwestward oriented rain belt over the west coast of Sumatra parallel to the local topography (see Figure 1) gradually migrates southwestward into the neighboring waters after 23LT. This propagating diurnal precipitation belt has been previously reported and linked to gravity wave propagation (e.g., Love et al., 2011; Yang & Slingo, 2001b). Meanwhile, precipitation over the MC land is largely suppressed in the early morning.

During the suppressed MJO period (Figure 3b), while precipitation over the EIO is persistently suppressed, the main features of the diurnal cycle of precipitation over the MC during the enhanced MJO phase can also be discerned, including the afternoon precipitation peak over the land and the prevalence of precipitation

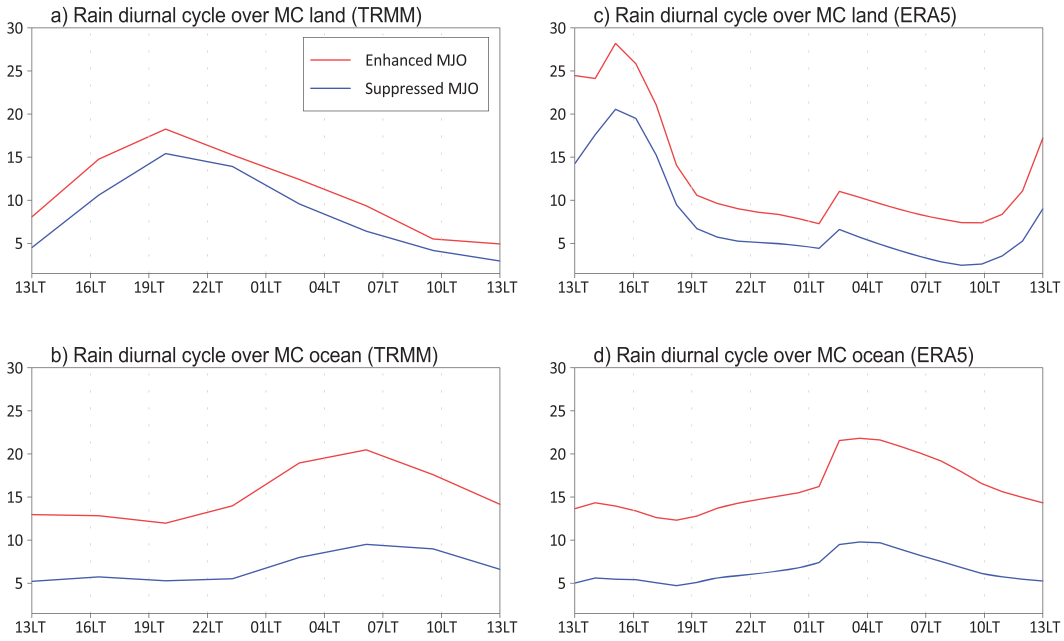

Figure 5. Composite diurnal cycle of precipitation (unit: mm day^{-1}) over the land (upper panels) and ocean (lower panels) of the MC area (95–119°E; 6°S to 6°N; see the rectangle box in the upper-left panel of Figure 3) based on TRMM (left) and ERA-5 (right) for the enhanced (red) and suppressed (blue) MJO phases over the EIO.

over the ocean in the local morning. A striking difference in the diurnal cycle between the enhanced and suppressed MJO phases, however, is that the migrating rain belt over west Sumatra is significantly weakened in the local morning during the suppressed MJO periods. This will be further discussed below.

Figure 4 illustrates diurnal precipitation evolution over the EIO and the MC during the enhanced and suppressed MJO periods based on the ERA-5 reanalysis. The most prominent features of the diurnal cycle as shown based on TRMM are largely captured in ERA-5, including the diurnal phases of precipitation over both the MC land and ocean as well as the greatly weakened offshore rain belt in the local morning over west Sumatra during the suppressed MJO periods. However, the maximum precipitation over the MC land is discerned between 14LT and 17LT in ERA-5, rather than the evening precipitation maximum in TRMM. Meanwhile, the southeast-northwestward oriented rain belt over west Sumatra during the enhanced MJO periods largely keeps stationary off the coast in ERA-5, in contrast to slow southwestward migration from land to offshore waters by TRMM. This indicates that the ECMWF IFS has difficulties in representing the detailed evolution of gravity waves and local land-sea breezes associated with the observed migrating rain belt over west Sumatra. Further analysis based on ERA-5 suggests that the greatly enhanced early-morning precipitation off the west Sumatra coast during the enhanced MJO phase is due to strengthening of low-level convergence by westerly anomalous MJO winds associated with the active MJO convection over the EIO (figure not shown).

The diurnal cycle of precipitation over the MC land and ocean during the two opposite MJO phases is further illustrated in Figure 5. With a main focus on the diurnal cycle over the western MC, each composite diurnal rainfall profile in Figure 5 is derived by averaging over corresponding land or ocean grids in the rectangular area in Figure 3 (95–119°E; 6°S to 6°N). Peak precipitation over the MC land is observed around 20LT by TRMM during both the enhanced and suppressed MJO periods (Figure 5a), with persistently stronger precipitation during the enhanced MJO periods throughout the day but with largely similar diurnal amplitude. The afternoon/early evening precipitation peak over the MC land is also noted in ERA-5, although it occurs at an earlier time around 15LT instead of 20LT in TRMM as previously discussed in Figure 4. Also, the reanalysis-based precipitation shows an abrupt decrease in the afternoon from 16LT to 19LT. Nevertheless, a largely similar diurnal precipitation amplitude during the enhanced and suppressed MJO phases and the systematically stronger precipitation over the entire day during the enhanced MJO periods over the MC

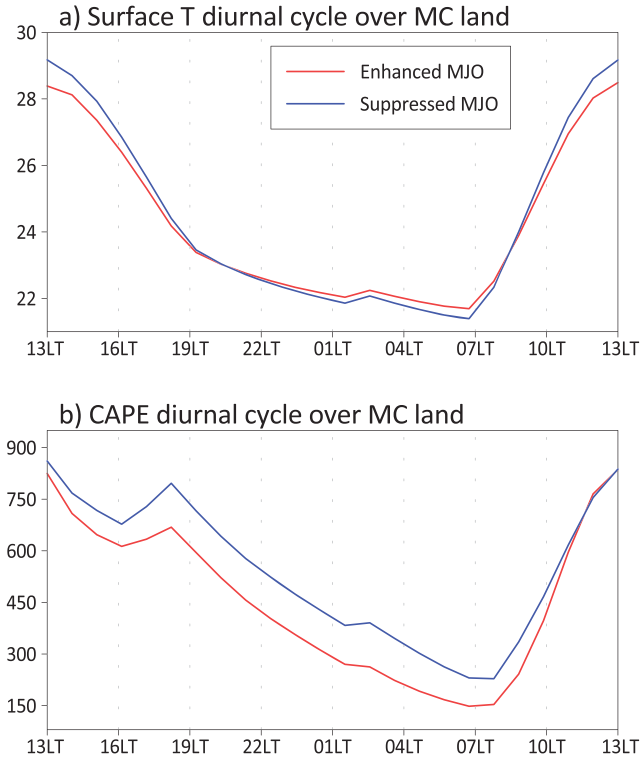

Figure 6. Similar to Figure 5, but for composite diurnal cycle of (a) surface temperature (units: °C) and (b) CAPE (J kg^{-1}) over the MC land based on ERA-5.

land are well represented in the ERA-5 reanalysis. This suggests that when the MJO convection is located over the EIO, the diurnal precipitation amplitude over the west MC land does not significantly change, but with increased daily mean precipitation possibly by the large-scale low-level convergence associated with the enhanced MJO convection. This result slightly differs from those previously reported that the diurnal cycle of rainfall tends to be enhanced over the MC land when the MJO convection is located over the Indian Ocean, for example, during the MJO phase 3 (Oh et al., 2012; Peatman et al., 2014). The plausible reason for this discrepancy could be that the MJO phases defined by the Wheeler-Hendon MJO index is dominated by large-scale circulation anomalies instead of convection signals (e.g., Kiladis et al., 2013). Therefore, for each selected day of the MJO Phase 3, it may not be necessary that active MJO convection is present over the EIO. While the enhanced and suppressed MJO phases identified in this study are based on the intraseasonal convection anomalies over a small EIO box, corresponding to the MJO convective condition right before it propagates eastward into the MC as shown in the regressed rainfall pattern between day −3 and day 0 in Figure 2 (opposite for the suppressed MJO phase).

Over the MC ocean, the observed diurnal cycle of precipitation is well captured in ERA-5 during both MJO phases and suggests that the MJO significantly modulates both the daily mean and diurnal amplitude of precipitation. One deficiency in reanalysis precipitation is the slightly earlier occurrence of peak precipitation around 03LT versus 06LT in TRMM. Also, the increase of reanalysis precipitation in the morning is more abrupt than that in the observations, partially due to the lack of a propagation mechanism in generating the offshore precipitation belt over west Sumatra in the ECMWF IFS as previously discussed.

To further understand the processes associated with MJO modulations on the diurnal evolution of precipitation, Figure 6 displays diurnal cycle of surface temperature and the convective available potential energy (CAPE) over the MC land during the two MJO phases based on ERA-5. While surface temperature in the reanalysis is also subject to model deficiencies, direct constraints from various in situ observations make it more reliable than the model precipitation. Pronounced diurnal variations in land surface temperature, with a maximum near 13LT and a minimum near 07LT, are evident during both the enhanced and suppressed

MJO periods, in agreement with largely similar diurnal precipitation amplitudes during both MJO periods. A slightly lower surface temperature in the afternoon and higher temperature in the early morning, thus a slightly weaker diurnal cycle of surface temperature, is discerned during the enhanced MJO phase over the MC land, possibly due to the associated stronger daily mean precipitation (Figure 5c). In contrast to the higher daily mean precipitation during the enhanced MJO phase, smaller values in CAPE are found over the MC land (Figure 6b), suggesting that the weakly enhanced daily mean precipitation over the MC land during the enhanced MJO periods could be promoted by large-scale convergence associated with active MJO convection rather than the local atmospheric instability.

To summarize, analyses in this section suggest that during the period of enhanced MJO convection over the EIO, while precipitation over the MC land is enhanced throughout the day compared to that during the suppressed MJO period, its diurnal amplitude and phase do not significantly change between these two MJO phases. Meanwhile, pronounced modulations of the daily mean as well as the diurnal amplitude of precipitation by the MJO are found over the MC oceans. These results may indicate that the upscale influences of the subdaily processes over the MC land may not play a dominant role in generating the local damping effect for the MJO. This will be further discussed in the following.

5. Key Processes Responsible for the MC Damping Effect for the MJO

In many recent studies, evolution of MJO convection has been closely linked to atmospheric moisture perturbations (e.g., Adames & Kim, 2016; Jiang, 2017; Raymond & Fuchs, 2009; Sobel & Maloney, 2012). In this section, based on a moisture budget analysis, we attempt to identify the essential processes responsible for the damped MJO amplitude over the MC land as shown in both TRMM and ERA-5 (Figure 2). Figure 7a shows a longitude-pressure cross-section of the anomalous specific humidity pattern at day −3 based on lag regression against 20–80 day filtered precipitation over the EIO box (85–95°E; 5°S to 5°N) based on ERA-5. Note that when deriving the regression patterns of 3D variables (winds, moisture, moisture tendency, etc.), due to a huge volume of the 3D data, these 3D variables are only subject to the removal of the climatological annual cycle (annual mean plus three leading annual harmonics) before regressed onto the 20–80 day filtered rainfall index over the EIO. The statistical significance of these 3D regression patterns is similarly assessed by their corresponding correlation coefficients, with the effective DOF at each grid estimated using both lag-one autocorrelations of each corresponding 3D variable and the EIO rainfall index following Bretherton et al. (1999).

To demonstrate a sharp influence of the topography over the MC on the MJO moisture profile, the cross-section is taken at the latitude of 3°S instead of averaging over equatorial latitudes. Associated with the enhanced MJO convection over the EIO at day −3 (see Figure 2 and labeled by the red solid triangle in Figure 7a), positive moisture anomalies are evident in the free atmosphere above 950 hPa (Figure 7a). A sharp reduction of positive moisture anomalies to the east of the mountain peak over Sumatra is readily seen, indicative of a significant impact of the MC topography on the MJO. Note that MC topographic effects on MJO moisture fields are evident in the entire lower troposphere up to 700 hPa, well beyond the altitude of the local mountain peak. Strong modulations of MJO moisture anomalies by Sumatra Island are again clearly discerned by the spatial distribution of 900–700 hPa averaged anomalous moisture pattern at day −3 (Figure 7c).

Figure 7b further displays moisture tendency anomalies at day −3 based on the same regression approach. Corresponding to the MJO convection center near 87°E at day −3, positive moisture tendencies (i.e., moistening) are largely found to the east of MJO convection associated with easterly anomalous winds (see Figure 7a), with lower-tropospheric moistening over a large portion of the MC region, signaling the preconditioning for the eastward propagation for the MJO (e.g., Benedict & Randall, 2009; Jiang et al., 2011; Johnson et al., 1999; Kemball-Cook & Weare, 2001; Tian et al., 2010). Interestingly, between the strong deep moistening over the EIO and shallow moistening over the eastern part of the MC, a lack of moistening is noted over Sumatra right to the east of the local mountain peak (100–105°E; Figure 7b), indicating an interruption of moistening process over Sumatra. The influence of MC topography on the MJO moistening can be further clearly illustrated by the spatial pattern of 900–700 hPa averaged moisture tendency anomalies at day −3 (Figure 7d). It is readily seen that the moistening in the lower troposphere to the east of MJO convection, which has been suggested critical for the eastward propagation of the MJO, is significantly

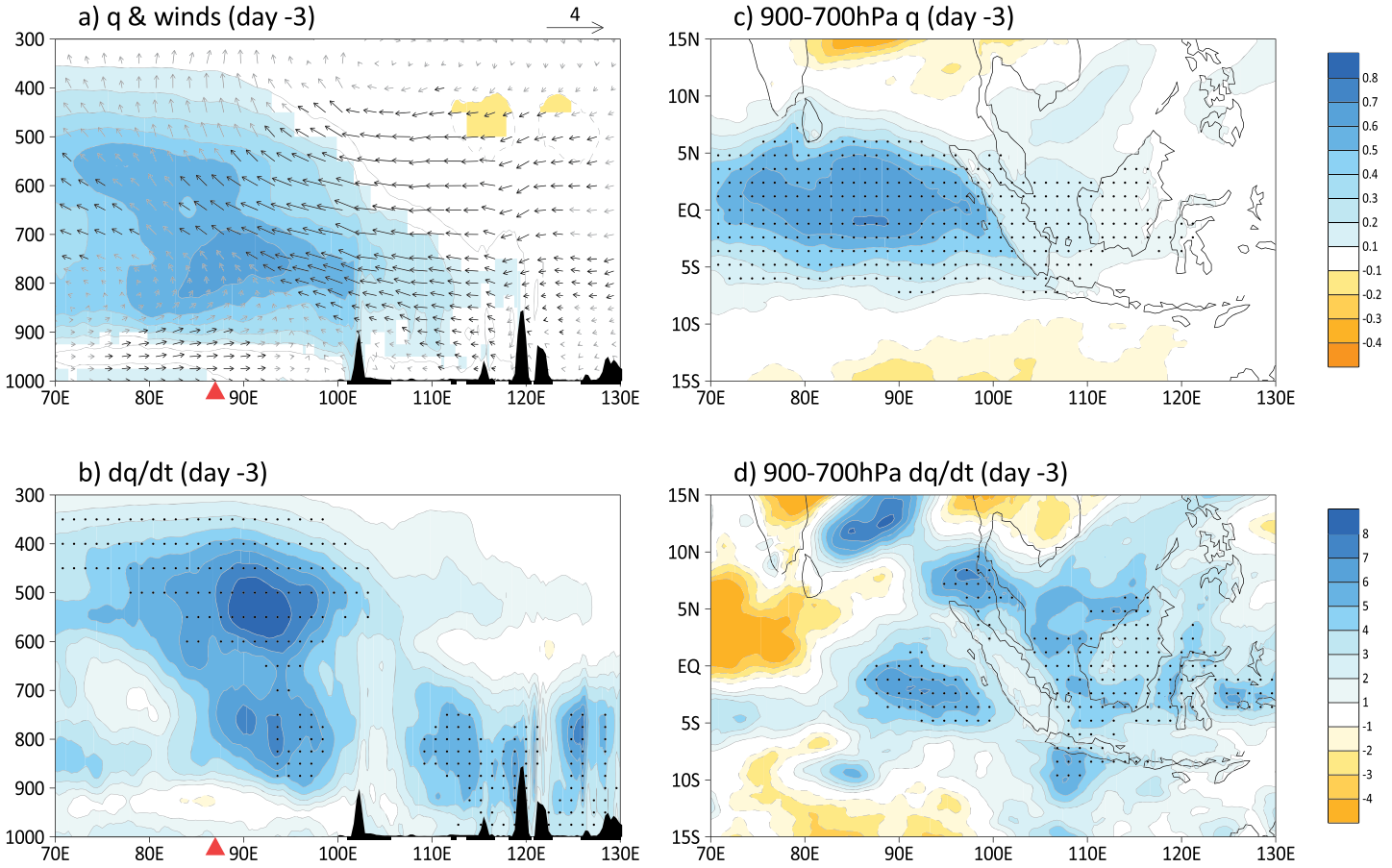

Figure 7. (Left panels) Longitude-pressure profiles of (a) moisture (shaded: g kg^{-1}) and u-w winds (vectors; see the scale on the upper-right with the unit of m s^{-1} for u-wind, and −15 Pa s^{-1} for vertical velocity). Only q anomalies that pass 95% significance level are plotted as shaded contours, and vectors with dark color represent where u-wind anomalies are statistically significant at 95% level; and (b) moisture tendency anomalies (unit: 10^{-10} g kg^{-1} s^{-1}) at 3°S. Black shading on the bottom of both panels denote topography over the MC; (right panels) spatial patterns of regressed 900–700 hPa averaged (c) moisture and (d) moisture tendency anomalies. In (b) to (d), grids where valuables are significant at 95% level are stippled. All fields are based on. All fields are derived by lag regressions onto the 20–80 day filtered precipitation over the EIO based on the ERA-5 reanalysis at day −3.

modulated by the MC islands. Strong moistening to the east of MJO convection is largely observed over the MC ocean region, in contrast to rather weak moistening over the MC land (Figure 7d). As the area of the MC land is comparable to that of the enhanced MJO convection (see Figure 2), it is expected that when MJO convection propagates into the MC, the damped MJO convection over the MC land will effectively destroy the previously well-organized MJO convection and associated circulation, and thus lead to an abrupt break down of MJO convection over the MC region as seen in Figure 2. Therefore, understanding the key processes responsible for the interruption of low-level moistening over the MC land as shown in Figures 7b and 7d will provide critical insights into the damping effect of the MC on the MJO eastward propagation. In the following, this will be explored by performing a moisture budget analysis associated with the MJO with a particular focus on the interruption of low-level moistening over Sumatra and Borneo.

The local time rate of change of specific humidity can be written as

$$\partial q/\partial t = -\overrightarrow{v}\cdot\nabla q - \omega(\partial q/\partial p) - Q_2/L_v, \quad (1)$$

where the terms on the right-hand side are, respectively, the horizontal and vertical moisture advection and the apparent moisture source and sink Q_2 as defined in Yanai et al. (1973), which represents the combined effects of evaporation and condensation within the column and the flux of moisture by unresolved eddies (Johnson et al., 2015; Yanai & Johnson, 1993). Since Q_2 is not directly archived by ERA-5, and also there

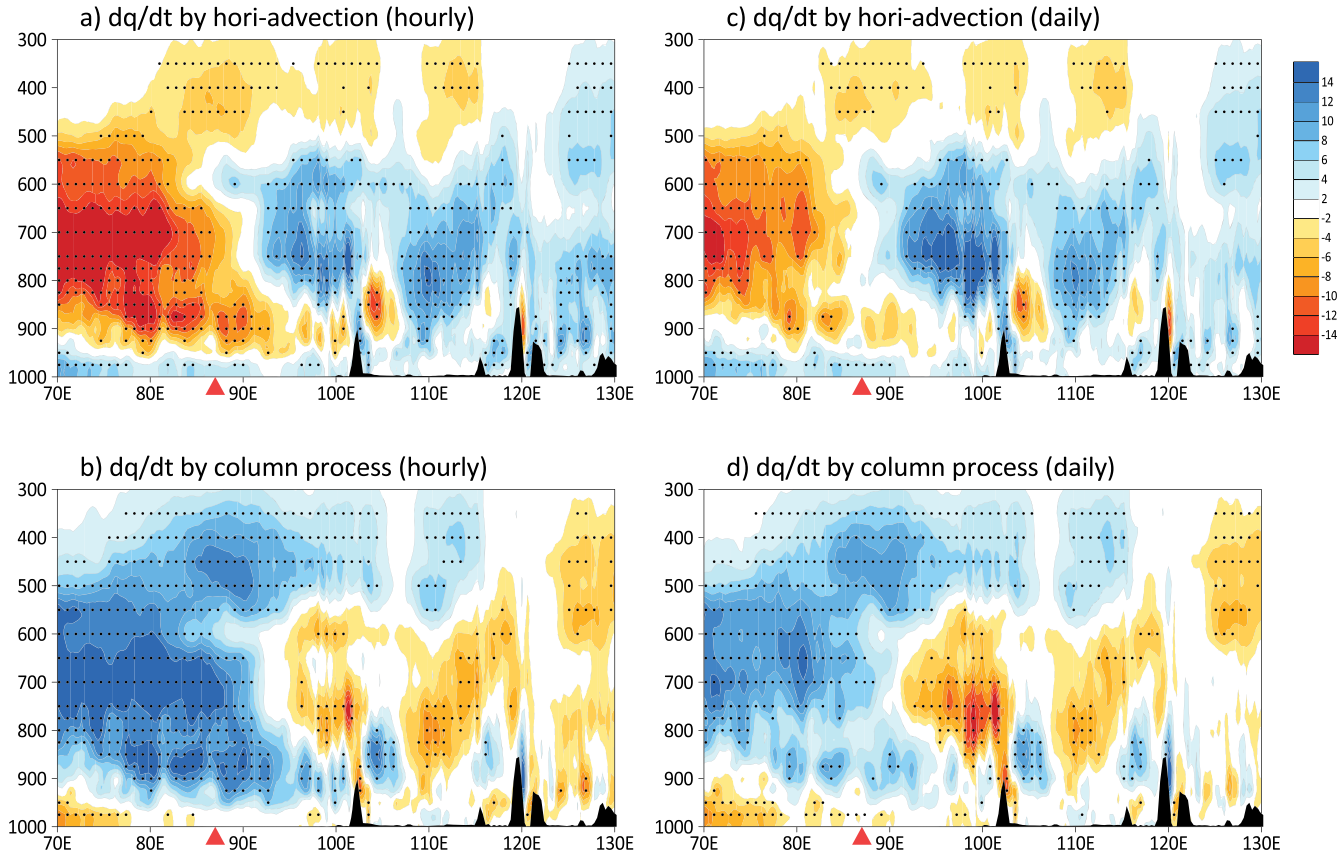

Figure 8. Longitude-pressure profiles of moisture tendency (unit: 10^{-10} g kg^{-1} s^{-1}) by the horizontal advection (upper panels) and the column processes (lower-panels). Patterns on the left (right) are derived based on hourly (daily) mean wind and moisture fields from the ERA-5 reanalysis. All fields are obtained by the lag regressions against IO precipitation at day −3 and averaged between 5°S and 5°N. Black shading in each panel denotes topography over the MC. Grids where moisture tendency anomalies are statistically significant at 95% level are stippled.

is a near cancellation between the vertical moisture advection and Q_2, the second and third terms on the right-hand side are combined and referred to as the column process following Chikira (2014) and Wolding et al. (2016). Daily moisture tendency due to the column process can be derived based on equation (1) given $\partial q/\partial t$ and $-\overrightarrow{v}\cdot\nabla q$ from the ERA-5 reanalysis, and its anomalous pattern associated with the MJO can be derived by regression onto the EIO precipitation as previously discussed. By taking advantage of the hourly output from ERA-5, the horizontal and vertical moisture advection will be calculated at hourly intervals, and then daily mean advection can be obtained based on these hourly data, which includes the upscale impact of subdaily systems on MJO moisture processes. Similarly, daily mean moisture advection associated with the MJO can also be calculated by using daily mean wind and specific humidity fields. Contributions to the MJO moisture transport due to diurnal processes can then be estimated by the differences of the horizontal/vertical moisture advection terms derived by hourly and daily wind and specific humidity fields.

To illustrate the processes responsible for the rather weak moistening over the MC land compared to neighboring ocean areas as illustrated in Figures 7b and 7d, the left panels in Figure 8 show moisture tendency profiles due to horizontal advection (Figure 8a) and the column process (Figure 8b) derived by hourly wind and specific humidity fields at day −3. Corresponding to the MJO convection near 87°E at this time (see the red solid triangle), the horizontal moisture advection is largely characterized by lower-tropospheric moistening to the east, and drying to the west of the MJO convection (Figure 8a), in accord with previous studies on the role of horizontal moisture advection in promoting the MJO eastward propagation over the IO (e.g., Maloney, 2009; Maloney et al., 2010; Andersen and Kuang, 2012; Sobel et al., 2014; Chikira, 2014; DeMott et al., 2014; Adames & Wallace, 2015; Arnold and Randall 2015; Jiang, 2017; Gonzalez & Jiang, 2017;

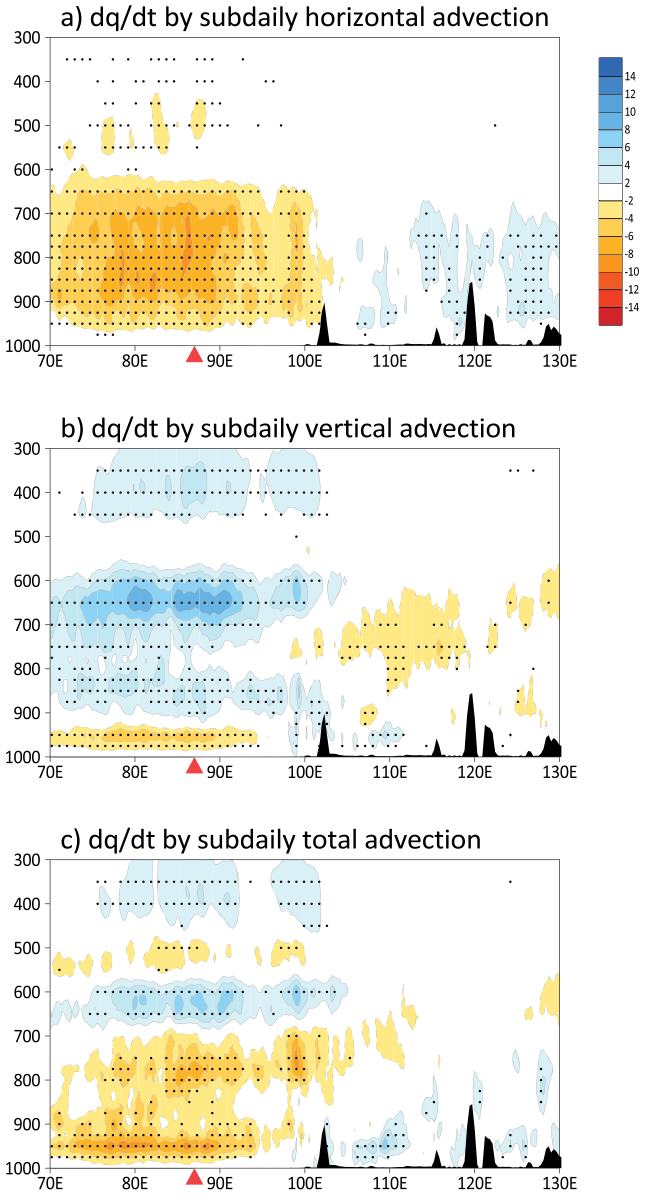

Figure 9. Contribution of subdaily processes for the horizontal (a), vertical (b), and total (c) moisture advection as estimated by differences in corresponding lag-regressed fields derived by hourly and daily mean reanalysis at day −3 and are averaged between 5°S and 5°N. Grids where moisture tendency anomalies are statistically significant at 95% level are stippled. The units are 10^{-10} g kg^{-1} s^{-1}.

Gonzalez & Jiang, 2019). An exception, however, is noted over Sumatra (near 105°E) right to the east of the local mountain peak, with a drying patch between 950 and 700 hPa while moistening prevails in the lower troposphere on both sides. The moisture tendency by the column process (Figure 8b) is largely in an opposite sign to the horizontal advection. Over the MJO convectively active region in the EIO (cf. Figure 2 right panels at day −3), the column process is largely moistening the atmosphere, that is, destabilizing the MJO convection, or a negative value of the effective gross moist stability (GMS), in support of the moisture mode theory (e.g., Benedict et al., 2014; Chikira, 2014; Jiang et al., 2015; Raymond et al., 2009; Raymond & Fuchs, 2009; Sobel & Maloney, 2013; Wolding et al., 2016). Over the MC region, the moisture tendency by the column process largely leads to a weak drying effect in association with local suppressed MJO convection. However, moistening is observed over Sumatra due to the column process, which largely offsets the local drying effect by the horizontal advection (Figure 8a), leading to a rather weak total moisture tendency over Sumatra (Figure 7b). Therefore, the interruption of MJO moisture preconditioning over Sumatra tends to be closely linked to the local drying effect by the horizontal moisture advection. While these above discussions mainly focus on Sumatra Island, relatively weaker drying tendencies due to the horizontal advection can also be observed in the lower troposphere over other MC islands (Figure 8a). Further understanding of the drying effect by the horizontal moisture advection over the MC islands, therefore, will help to understand the damping effect of the MC for the MJO propagation.

As previously discussed, the role of diurnal moisture transport on the MJO moisture tendency can be evaluated by comparing moisture tendency profiles derived from hourly wind and q fields (Figures 8a and 8b) to those based on daily data (Figures 8c and 8d). Differences between the right and left panels in Figure 8 thus represent the role of diurnal moisture transport for the MJO and are shown in Figure 9. A quick comparison of Figures 8a and 8c suggests that the diurnal moisture transport is not essential for the formation of the lower-tropospheric drying over Sumatra and other MC islands through the horizontal advection. As shown in Figure 9a, horizontal moisture transport by subdaily processes is largely characterized by a weak low-level moistening (drying) over the IO (MC region) where MJO convection is enhanced (suppressed). Meanwhile, the diurnal vertical moisture transport is largely confined over the IO associated with the enhanced MJO convection, with moistening in the free atmosphere and drying in the planetary boundary layer (PBL; Figure 9b). As a result, the total effect by the diurnal horizontal and vertical transport leads to a cancellation between each other (Fig 9c). Over the MC, the total subdaily moisture transport contributes to a weak moistening in the PBL, but with rather weak impacts in the lower troposphere.

Since the moisture tendency due to the horizontal advection derived by daily data as shown in Figure 8c well captures the low-level drying effect over Sumatra and other MC islands corresponding to enhanced MJO convection over the EIO at day −3, analyses in the following will mainly focus on the horizontal moisture advection using daily wind and specific humidity. Decomposition of the total horizontal moisture advection into zonal and meridional components suggests that the aforementioned low-level drying over the MC islands is largely due to the zonal advection (cf. Figures 10a and 8c). In order to identify the detailed processes leading to this drying effect, further diagnosis is performed by separating daily zonal-wind (u-wind) and specific humidity into three different time scales following previous studies (e.g., Gonzalez & Jiang,

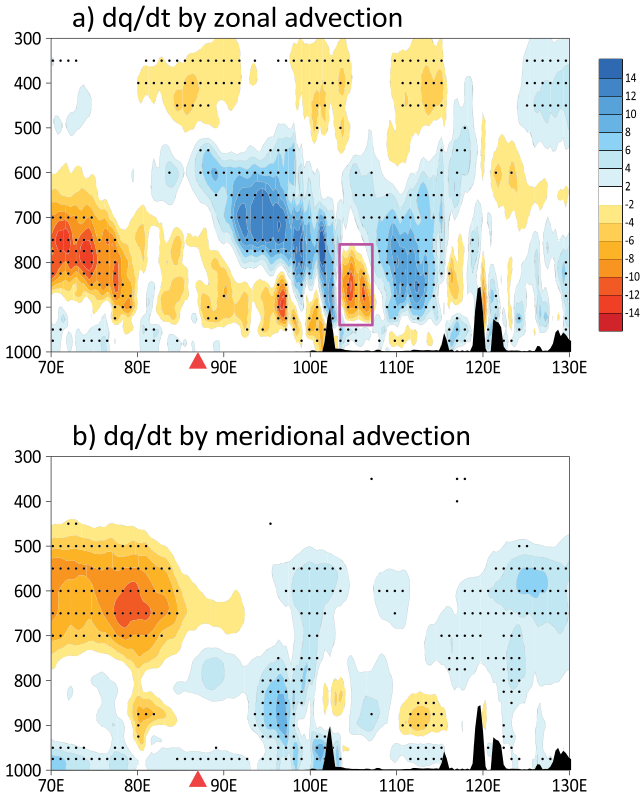

Figure 10. Similar as in Figure 9, but for longitude-pressure profiles of moisture tendency (unit: 10^{-10} g kg^{-1} s^{-1}) by the zonal (a) and meridional (b) advection at day −3, derived by daily u-wind and moisture fields based on ERA-5.

2019; Jiang, 2017), that is, low-frequency (period >100 day, with mean seasonal cycle included), intraseasonal (MJO; 20–100 day), and high-frequency (<20 day) time scales. By firstly focusing on the drying process over Sumatra (the pink box in Figure 10a), Figure 11 shows the total low-level moisture tendency by the zonal advection along with contributions by nine advection terms with a combination of u-wind and q at different time scales. Contribution of the zonal moisture advection due to subdaily processes, estimated by differences in values calculated by hourly and daily data as previously described, is also shown in Figure 11. It is clearly seen that the drying effect over Sumatra by the total zonal moisture advection at day −3 is mainly due to the advection of low-frequency moisture by the MJO anomalous zonal winds, for example, through the term of $-u' \frac{\partial q_m}{\partial x}$.

The vertical-longitudinal cross-section of the moisture tendency due to $-u' \frac{\partial q_m}{\partial x}$ at day −3 is further displayed in Figure 12a. Alternating moistening and drying structures in the lower troposphere over the EIO and MC region are readily seen. Particularly interesting is that this moisture tendency pattern exhibits a clear spatial lock to the MC mountains, with drying (moistening) tendencies located to the east (west) side of mountain peaks. Figure 12b further illustrates spatial distribution of 900–750 hPa vertically averaged moisture tendency by $-u' \frac{\partial q_m}{\partial x}$. Regulation of moisture tendency over the major MC islands by local topography is again clearly evident. Given easterly anomalous winds in the lower troposphere over the MC associated with active MJO convection over the EIO at day −3 (vectors in Figure 12c; also, see Figure 7a), the spatial lock of the moisture tendency pattern by $-u' \frac{\partial q_m}{\partial x}$ to the local mountains is mainly due to collocation of the maximum low-frequency or seasonal mean moisture (q_m) over the MC mountain peaks (see shaded contours in Figure 12c, and cf. Figure 1). Advection of this seasonal mean moisture pattern by the easterly anomalous MJO winds gives rise to low-level drying (moistening) to the east (west) side of mountain peaks. Over Sumatra, because the mountain is located over the western edge of the island (Figure 1), the drying effect prevails over a large portion of the island (Figure 12b), in agreement with a strong drying patch over Sumatra in the vertical profiles of the

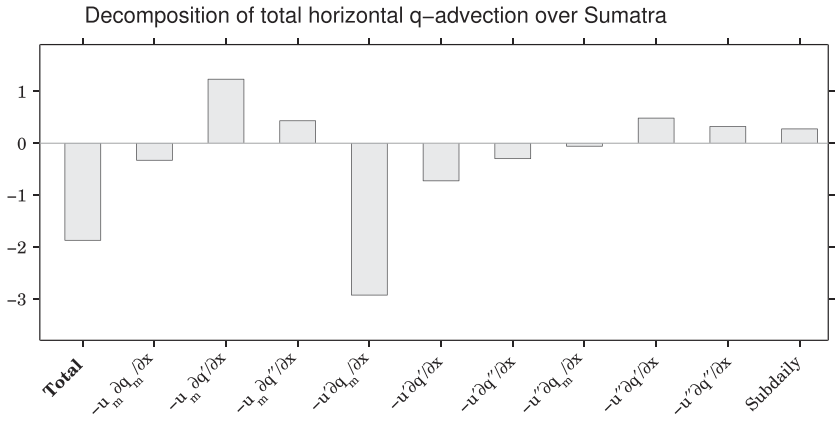

Figure 11. Decomposition of the drying effect (unit: 10^{-10} g kg^{-1} s^{-1}) due to the lower-tropospheric horizontal moisture advection over Sumatra (the rectangular box in Figure 10a) into processes due to different time scales, that is, low-frequency variability with a period greater than 100 days (denoted by the subscript "m"), MJO time-scale with a period between 20 and 100 days (denoted by a prime), and high-frequency variability with a period shorter than 20 days (denoted by a double prime). Contribution by subdaily processes, estimated by differences in values calculated by hourly and daily data, is also shown.

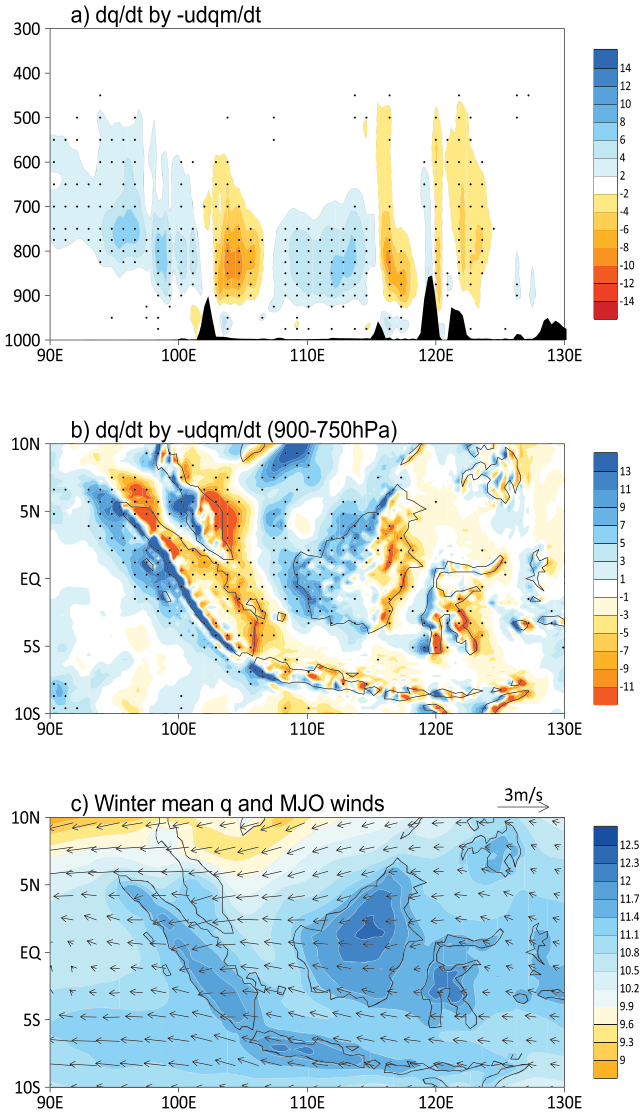

Figure 12. (a) Similar as in Figure 10, but for moisture tendency (unit: 10^{-10} g kg^{-1} s^{-1}) by zonal advection of the seasonal mean moisture by anomalous MJO winds ($-u' \frac{\partial q_m}{\partial x}$). Grids where values are statistically significant at 95% level are stippled; (b) 900–750 hPa vertically averaged $-u' \frac{\partial q_m}{\partial x}$ pattern (unit: 10^{-10} g kg^{-1} s^{-1}); (c) 900–750 hPa vertically averaged winter mean moisture (shaded; unit: g kg^{-1}) and MJO anomalous winds (vectors with the scale on the upper-right of the panel).

total horizontal moisture advection term (Figure 8). While the north-south oriented mountain peaks are situated over the center of Borneo, low-level drying is observed over the eastern part of the island, while moistening over west Borneo and part of the ocean area between Sumatra and Borneo (Figure 12b). Interestingly, the largely drying over Sumatra, as well as the east-west drying/moistening dipole over Borneo at day −3, is closely linked to the anomalous MJO precipitation pattern over these islands in the following days in both TRMM and ERA-5 (e.g., day 3 in Figure 2), which provides further evidence on the critical role of the zonal moisture advection for the MJO damping effect over the MC lands. Note that given a fixed mean moisture pattern, the damping effect through this moisture advection process is linearly corresponding to MJO amplitude. For a stronger (weaker) MJO event over the IO, the induced drying over the MC lands is also expected to be stronger (weaker) due to stronger (weaker) MJO anomalous circulation. Therefore, this process does not indicate that stronger MJO events tend to more easily cross over the MC than weaker ones.

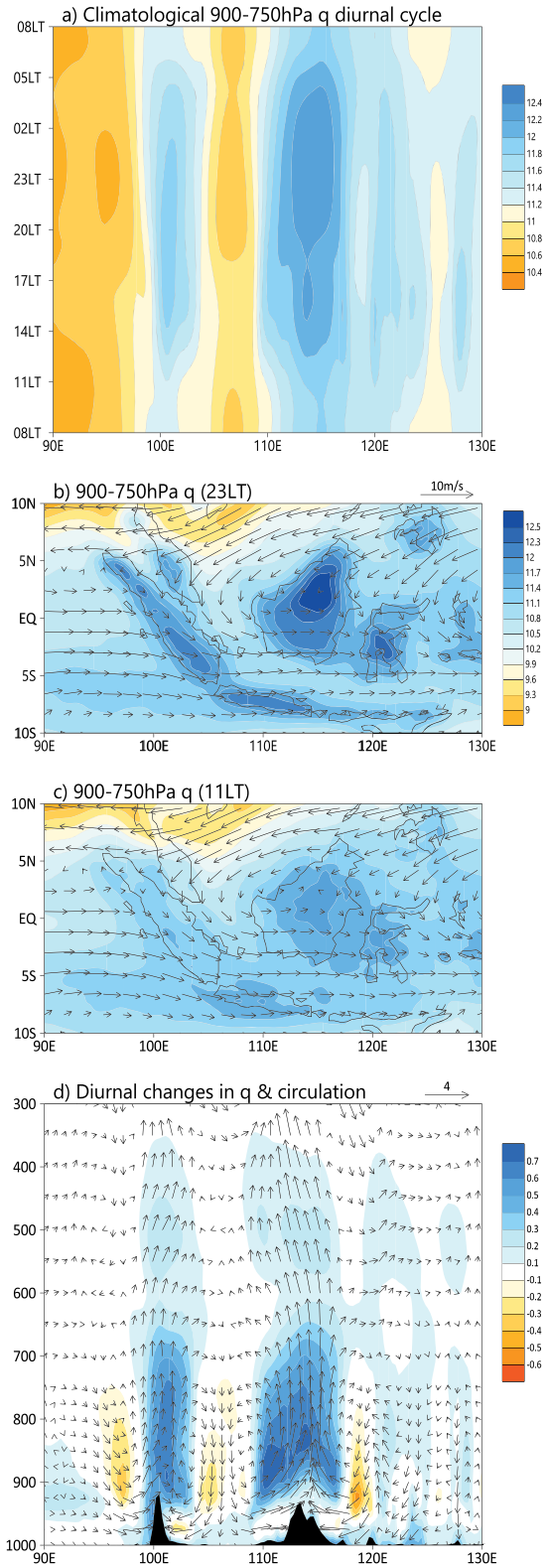

Figure 13. (a) Diurnal local time versus longitude evolution of 900–750 hPa averaged winter mean moisture over 5°S to 5°N latitude belts; and spatial patterns of 900–750 hPa vertically averaged winter mean moisture (shaded) and winds (vectors; see the scale on the upper-right of panel (b) at local time 23LT (b) and 11LT (c); (d) longitude-pressure profiles of the differences in winter mean moisture (shaded) and u-w winds (see the scale on the upper-right of panel (d) with the unit of m s^{-1} for u-wind, and −15 Pa s^{-1} for vertical velocity) between 23LT and 11LT. Units for the specific humidity fields are g kg^{-1} in all panels.

The topographically locked horizontal moisture advection patterns over the MC associated with the MJO were also reported in several previous studies based on the ERA-Interim reanalysis and climate model simulations (e.g., DeMott et al., 2014; Hung & Sui, 2018). Particularly, based on a moisture budget analysis for the MJO over the MC using daily ERA-Interim reanalysis, Hung and Sui (2018) also suggested that advective moistening over the MC region tends to be negative (positive) on the east (west) side of the major MC islands, which could interrupt the MJO eastward propagation over the MC land and be conducive to a southward detour of the eastward-propagating MJO as previously proposed (Kim et al., 2017). By employing high-resolution ERA-5 reanalysis in this study, a strong spatial lock of the low-level seasonal mean moisture pattern to local mountains over the MC is further clearly illustrated. Meanwhile, the hourly output of the ERA-5 reanalysis used in this study provides a great opportunity to examine how diurnal processes contribute to the interruption of low-level moistening over the MC during MJO eastward propagation. A local time versus longitude (5°S to 5°N averaged) evolution diagram of the climatological winter mean 900–750 hPa specific humidity suggests that the low-level winter mean moisture exhibits a strong diurnal evolution over the MC land with maxima during the late afternoon and early evening (Figure 13a), but a much weaker diurnal cycle over the ocean. As a result, a strong horizontal gradient in the low-level moisture pattern is observed during the local evening, closely following the shape of local topography (Figure 13b), while a rather weak moisture gradient in the morning (Figure 13c). The enhanced low-level moisture over the MC mountains during the local evening is closely associated with strong diurnal upslope winds as shown in Figure 13d, which is in accord with previous studies (e.g., Qian, 2008). Further investigations, however, are needed to better understand the detailed processes in defining the seasonal mean moisture pattern over the MC. For example, the maximum rainfall over the MC land occurs in the local afternoon about 15LT (Figures 4 and 5c) based on ERA-5; it is not obvious why the maximum moisture forms during nighttime over the mountains. The vertical mixing associated with the diurnal cycle over the MC land could play a critical role in defining the local moisture profiles but is not available from the ERA-5 dataset. Meanwhile, large analysis increment in the reanalysis data (e.g., Jiang, 2017; Kiranmayi & Maloney, 2011; Mapes & Bacmeister, 2012) further makes it difficult to completely understand the detailed physical processes in regulating the diurnal variations in the seasonal mean moisture pattern. Diagnosis and sensitivity experiments based on high-resolution model simulations could provide important insights into the key factors regulating the local mean moisture profiles. Additionally, the diurnal cycle over the MC as suggested by ERA-5 will also need to be verified from in situ observations, for example, from the ongoing Years of the Maritime Continent (YMC) field campaign (https://www.jamstec.go.jp/ymc).

6. Summary and Discussions

While the MJO plays a significant role in the global hydrological cycle, realistic representation of the MJO in climate models has been challenging, mainly due to our limited understanding of processes regulating atmospheric convection. Organization of the MJO is further complicated by interactions among convective systems at various temporal and spatial scales, particularly when interfering with tropical mountains, for example, over the MC. The MC exerts a strong damping effect on eastward propagation of the MJO when propagating from the EIO to the western Pacific. This damping effect is often over-exaggerated in present-day climate models, limiting our prediction skill for the MJO and its impacts on downstream weather extremes beyond the MC. Despite various existing hypotheses, including the upscale impact of the diurnal cycle, the underlying physics of the MC damping effect on the MJO remains poorly understood, partially due to the lack of high-resolution observations and model inability to credibly represent the interaction between the MC and MJO.

In this study, we capitalize on the new high-resolution ERA-5 reanalysis to investigate the essential processes responsible for the damping of MJO amplitude over the MC land, including the role of the local diurnal cycle. Results based on both TRMM and ERA-5 suggest that both the amplitude and phase of the diurnal rainfall cycle over the MC land do not exhibit significant changes between the enhanced and suppressed MJO phases over the EIO, although persistent enhancement of precipitation is observed throughout the day during the enhanced MJO periods (Figures 5a and 5c). Over the MC ocean, particularly off the coast of west Sumatra, significant enhancement in amplitude of diurnal rainfall cycle, along with a persistent increase in daily mean precipitation, is observed during the enhanced MJO periods (Figures 5b and 5d).

Since the lower-tropospheric moisture has been found to be critical in regulating MJO convection, a moisture budget analysis is further conducted to unravel key processes for damped MJO convection when crossing over the MC. The MC topography is found to exert significant influences on anomalous MJO moisture pattern. When the enhanced MJO convection is located over the EIO, positive moisture anomalies, with maxima in the lower troposphere, are clearly evident over the EIO, but sharply reduced to the east of mountain peak over the west edge of Sumatra (Figures 7a and 7b). Meanwhile, the low-level moistening (positive moisture tendency) to the east of MJO convection, indicative of the moisture preconditioning process for MJO eastward propagation, is only evident over the ocean, while absent or rather weak over the MC islands including Sumatra and Borneo (Figure 7b and 7d). The lack of lower-tropospheric moisture preconditioning over the MC land, therefore, suggests unfavorable conditions for MJO development during its eastward propagation.

It is further illustrated that the interruption of low-level moistening over the MC land is mainly due to a drying effect induced by zonal moisture advection (Figure 12a), dominated by advection of the seasonal mean moisture by the MJO zonal wind in the lower troposphere (Figure 11). By using the high-resolution ERA-5 reanalysis, it is further illustrated that the low-level mean moisture pattern over the MC closely follows local terrains, with moisture maxima largely collocated with mountain peaks over Sumatra and Borneo (Figures 12 and 13). Given this mean moisture distribution, its advection by anomalous easterly MJO winds corresponding to the active MJO convection over the EIO induces a drying (moistening) effect to the east (west) of local mountain peaks (Figure 12). Diagnosis based on hourly data from ERA-5 suggests that the moisture transport due to subdaily processes does not play an essential role in contributing the interruption of MJO moisture preconditioning over the MC islands. The diurnal cycle, however, can also be critical for the above mentioned MC damping effect for the MJO through its pronounced modulation on the seasonal mean moisture distributions over the MC islands (Figure 13).

These results indicate that the topography over the major MC islands plays a critical role in interrupting the eastward propagation of the MJO by shaping the spatial distribution of the lower-tropospheric mean moisture pattern. In particular, as the mountain peaks on Sumatra is located near the west edge of the island and straddle the equator between 5°S and 5°N, the zonal moisture advection as mentioned above will generate a drying effect over a great portion of Sumatra (Figure 12b) and thus effectively inhibits MJO eastward propagation. Over Borneo, since the north-south oriented mountain ridges are largely situated in the center of the island, the drying effect due to the horizontal moisture advection is confined to the eastern part of the island, while moistening occurs over west Borneo as well as the ocean region between Sumatra and Borneo. Interestingly, rather weak (strong) intraseasonal rainfall variability in general over the eastern (western) part of Borneo is also observed in the intraseasonal rainfall variance pattern (e.g., see Figure 1 from Sobel et al., 2008), lending further confidences on the critical role of MC topography in regulating the local MJO variability. The strong intraseasonal variability observed over west Borneo, on the other hand, indicates that the lack of latent heat flux over the MC land as previously proposed (e.g., Sobel et al., 2008; Sobel et al., 2010) may only be partially responsible for the damped MJO amplitude over the MC.

Therefore, GCMs that are unable to realistically depict the mean moisture pattern over the MC, either due to coarse model resolution to fully resolve MC topography or model deficiencies in representing the local diurnal cycle, could have difficulties in representing the interaction between the MJO and MC. It is also possible that great sensitivity of simulated MJO propagation and variability over the MC to the diurnal cycle (Hagos et al., 2016) and model surface evapotranspiration (Lee et al., 2012) as previously reported could be associated with the modified low-level mean moisture distribution over the MC due to changes of the model processes. Further investigations will be needed to better understand key processes for the formation of maximum low-level moisture over MC mountains, for example, through detailed diagnoses based on GCM simulations and model sensitivity experiments by modifying the location and orientation of the MC mountains. While the analyses in this study mainly focus on the west MC region, role of topography over the east MC for the MJO, for example, New Guinea, will also need to be explored. Moreover, the processes underlying the MC damping effect for MJO propagation as illustrated in this study are applicable for all MJO events crossing over the MC; further investigations are warranted to understand mechanisms responsible for the observed distinct MJO propagation characteristics over the MC; that is, some MJO events can cross over the MC, while others cannot. It will be interesting to further explore how interactions between the MJO and MC are modulated by the large-scale environment, for example, through the lower-tropospheric mean moisture distribution (e.g., DeMott et al., 2018; Gonzalez & Jiang, 2019; Kim, Kug, & Sobel, 2014) and

diurnal cycle-related local land-sea contrast (e.g., Ling et al., 2019; Zhang & Ling, 2017), as previously found to be critical in regulating propagating versus nonpropagating MJO events over the MC. Also note that in addition to the moistening process as discussed in this study, the MC diurnal cycle can also interact with the MJO through upscale transport of momentum and heat, which will be reported elsewhere.

While the high-resolution hourly ERA-5 reanalysis provides an unprecedented dataset to investigate key processes associated with the MC damping effect for the MJO, particularly on the role of the diurnal cycle, deficiencies in ERA-5 are also noted. For example, in TRMM observations, diurnal convective systems gradually migrate from the west Sumatra coast to neighboring oceans in the early morning. In contrast, the movement of convection systems are not well represented in ERA-5 although the morning peak of precipitation over the ocean off the west Sumatra coast is captured. The in situ observations from the ongoing YMC field project could therefore provide important validations of the ERA-5 reanalysis, including the detailed characteristics of the diurnal cycle of precipitation, circulation, and moisture profiles.

Acknowledgments
We thank three anonymous reviewers and the editor Chidong Zhang for their insightful comments. We also thank the NASA TRMM Project for providing TRMM3B42v7 3-hourly rainfall data and the ECMWF for providing the new-generation ERA-5 reanalysis. The TRMM rainfall data can be accessed online (https://disc.gsfc.nasa.gov/datasets/TRMM_3B42_7/summary). The ERA-5 data can be downloaded online (https://cds.climate.copernicus.eu/cdsapp#!/dataset/reanalysis-era5-pressure-levels). XJ acknowledges support by the NOAA Climate Program Office under awards NA15OAR4310098, NA15OAR4310177, and NA17OAR4310261. HS and DEW conduct the work in the Jet Propulsion Laboratory, under contract with NASA.

References

Adames, Á. F. (2017). Precipitation budget of the Madden-Julian Oscillation. *Journal of the Atmospheric Sciences*, *74*, 1799–1817. https://doi.org/10.1175/jas-d-16-0242.1

Adames, Á. F., & Kim, D. (2016). The MJO as a dispersive, convectively coupled moisture wave: Theory and observations. *Journal of the Atmospheric Sciences*, *73*, 913–941. https://doi.org/10.1175/JAS-D-15-0170.1

Adames, Á. F., & Wallace, J. M. (2015). Three-dimensional structure and evolution of the moisture field in the MJO. *Journal of the Atmospheric Sciences*, *72*, 3733–3754. https://doi.org/10.1175/JAS-D-15-0003.1

Ahn, M.-S., Kim, D., Sperber, K. R., Kang, I.-S., Maloney, E., Waliser, D., & Hendon, H. (2017). MJO simulation in CMIP5 climate models: MJO skill metrics and process-oriented diagnosis. *Climate Dynamics*, 1–23. https://doi.org/10.1007/s00382-017-3558-4

Baranowski, D. B., Waliser, D. E., Jiang, X., Ridout, J. A., & Flatau, M. K. (2019). Contemporary GCM fidelity in representing the diurnal cycle of precipitation over the Maritime Continent. *Journal of Geophysical Research:Atmospheres*, *124*, 747–769. https://doi.org/10.1029/2018JD029474

Benedict, J. J., Maloney, E. D., Sobel, A. H., & Frierson, D. M. W. (2014). Gross moist stability and MJO simulation skill in three full-physics GCMs. *Journal of the Atmospheric Sciences*, *71*, 3327–3349. https://doi.org/10.1175/JAS-D-13-0240.1

Benedict, J. J., & Randall, D. A. (2009). Structure of the Madden-Julian Oscillation in the superparameterized CAM. *Journal of the Atmospheric Sciences*, *66*, 3277–3296.

Birch, C. E., Webster, S., Peatman, S. C., Parker, D. J., Matthews, A. J., Li, Y., & Hassim, M. E. E. (2016). Scale interactions between the MJO and the western Maritime Continent. *Journal of Climate*, *29*, 2471–2492. https://doi.org/10.1175/JCLI-D-15-0557.1

Bretherton, C. S., Widmann, M., Dymnikov, V. P., Wallace, J. M., & Blade, I. (1999). The effective number of spatial degrees of freedom of a time-varying field. *Journal of Climate*, *12*, 1990–2009.

Chen, S. S., Houze, R. A., & Mapes, B. E. (1996). Multiscale variability of deep convection in relation to large-scale circulation in TOGA COARE. *Journal of the Atmospheric Sciences*, *53*, 1380–1409.

Chikira, M. (2014). Eastward-propagating intraseasonal oscillation represented by Chikira-Sugiyama cumulus parameterization. Part II: Understanding Moisture Variation under Weak Temperature Gradient Balance. *Journal of the Atmospheric Sciences*, *71*, 615–639. https://doi.org/10.1175/JAS-D-13-038.1

Dee, D. P., Uppala, S. M., Simmons, A. J., Berrisford, P., Poli, P., Kobayashi, S., et al. (2011). The ERA-Interim reanalysis: Configuration and performance of the data assimilation system. *Quarterly Journal of the Royal Meteorological Society*, *137*, 553–597. https://doi.org/10.1002/qj.828

DeMott, C. A., Stan, C., Randall, D. A., & Branson, M. D. (2014). Intraseasonal variability in coupled GCMs: The roles of ocean feedbacks and model physics. *Journal of Climate*, *27*, 4970–4995. https://doi.org/10.1175/JCLI-D-13-00760.1

DeMott, C. A., Wolding, B. O., Maloney, E. D., & Randall, D. A. (2018). Atmospheric mechanisms for MJO Decay over the Maritime Continent. *Journal of Geophysical Research: Atmospheres*, *123*, 5188–5204. https://doi.org/10.1029/2017jd026979

Duchon, C. E. (1979). Lanczos filtering in one and two dimensions. *Journal of Applied Meteorology*, *18*, 1016–1022.

ECMWF (2017). ERA5 reanalysis bt the European Centre for Medium-Range Weather Forecasts. Document of the dataset can be found at https://confluence.ecmwf.int/display/CKB/ERA5+data+documentation. Data downloaded from https://cds.climate.copernicus.eu/cdsapp#!/dataset/reanalysis-era5-pressure-levels

Fu, X., Lee, J.-Y., Wang, B., Wang, W., & Vitart, F. (2013). Intraseasonal forecasting of the Asian summer monsoon in four operational and research models. *Journal of Climate*, *26*, 4186–4203. https://doi.org/10.1175/JCLI-D-12-00252.1

Gonzalez, A. O., & Jiang, X. (2017). Winter mean lower-tropospheric moisture over the Maritime Continent as a climate model diagnostic metric for the propagation of the Madden-Julian Oscillation. *Geophysical Research Letters*. https://doi.org/10.1002/2016GL072430

Gonzalez, A. O., & Jiang, X. (2019). Distinct propagation characteristics of intraseasonal variability over the tropical West Pacific. *Journal of Geophysical Research: Atmospheres*, *0*, https://doi.org/10.1029/2018JD029884.

Hagos, S. M., Zhang, C., Feng, Z., Burleyson, C. D., De Mott, C., Kerns, B., et al. (2016). The impact of the diurnal cycle on the propagation of Madden-Julian Oscillation convection across the Maritime Continent. *Journal of Advances in Modeling Earth Systems*. https://doi.org/10.1002/2016MS000725

Hsu, H.-H., & Lee, M.-Y. (2005). Topographic effects on the eastward propagation and initiation of the Madden-Julian Oscillation. *Journal of Climate*, *18*, 795–809. https://doi.org/10.1175/JCLI-3292.1

Huffman, G. J., Adler, R. F., Rudolf, B., Schneider, U., & Keehn, P. R. (1995). Global precipitation estimates based on a technique for combining satellite-based estimates, rain-gauge analysis, and NWP model precipitation information. *Journal of Climate*, *8*, 1284–1295.

Hung, C.-S., & Sui, C.-H. (2018). A diagnostic study of the evolution of the MJO from Indian Ocean to Maritime Continent: Wave dynamics versus advective moistening processes. *Journal of Climate*, *31*, 4095–4115. https://doi.org/10.1175/jcli-d-17-0139.1

Inness, P. M., & Slingo, J. M. (2006). The interaction of the Madden-Julian Oscillation with the Maritime Continent in a GCM. *Quarterly Journal of the Royal Meteorological Society*, *132*, 1645–1667.
Jiang, X. (2017). Key processes for the eastward propagation of the Madden-Julian Oscillation based on multimodel simulations. *Journal of Geophysical Research: Atmospheres*. https://doi.org/10.1002/2016JD025955
Jiang, X., Waliser, D. E., Olson, W. S., Tao, W.-K., L'Ecuyer, T. S., Li, K.-F., et al. (2011). Vertical diabatic heating structure of the MJO: Intercomparison between recent reanalyses and TRMM estimates. *Monthly Weather Review*, *139*, 3208–3223. https://doi.org/10.1175/2011mwr3636.1
Jiang, X., Waliser, D. E., Xavier, P. K., Petch, J., Klingaman, N. P., Woolnough, S. J., et al. (2015). Vertical structure and physical processes of the Madden-Julian oscillation: Exploring key model physics in climate simulations. *Journal of Geophysical Research: Atmospheres*, *120*, 4718–4748. https://doi.org/10.1002/2014JD022375
Johnson, R. H., Ciesielski, P. E., Ruppert, J. H., & Katsumata, M. (2015). Sounding-based thermodynamic budgets for DYNAMO. *Journal of the Atmospheric Sciences*, *72*, 598–622. https://doi.org/10.1175/JAS-D-14-0202.1
Johnson, R. H., Rickenbach, T. M., Rutledge, S. A., Ciesielski, P. E., & Schubert, W. H. (1999). Trimodal characteristics of tropical convection. *Journal of Climate*, *12*, 2397–2418.
Kemball-Cook, S. R., & Weare, B. C. (2001). The onset of convection in the Madden-Julian Oscillation. *Journal of Climate*, *14*, 780–793.
Kerns, B. W., & Chen, S. S. (2016). Large-scale precipitation tracking and the MJO over the Maritime Continent and Indo-Pacific warm pool. *Journal of Geophysical Research: Atmospheres*, *121*, 8755–8776. https://doi.org/10.1002/2015JD024661
Kikuchi, K., & Wang, B. (2008). Diurnal precipitation regimes in the global tropics. *Journal of Climate*, *21*, 2680–2696. https://doi.org/10.1175/2007JCLI2051.1
Kiladis, G. N., Dias, J., Straub, K. H., Wheeler, M. C., Tulich, S. N., Kikuchi, K., et al. (2013). A comparison of OLR and circulation-based indices for tracking the MJO. *Monthly Weather Review*, *142*, 1697–1715. https://doi.org/10.1175/MWR-D-13-00301.1
Kiladis, G. N., Wheeler, M. C., Haertel, P. T., Straub, K. H., & Roundy, P. E. (2009). Convectively coupled equatorial waves. *Reviews of Geophysics*, *47*, RG2003. https://doi.org/10.1029/2008RG000266
Kim, D., Kim, H., & Lee, M.-I. (2017). Why does the MJO detour the Maritime Continent during austral summer? *Geophysical Research Letters*, n/a-n/a. https://doi.org/10.1002/2017GL072643
Kim, D., Kug, J.-S., & Sobel, A. H. (2014). Propagating versus nonpropagating Madden-Julian Oscillation events. *Journal of Climate*, *27*, 111–125. https://doi.org/10.1175/JCLI-D-13-00084.1
Kim, D., Sobel, A. H., & Kang, I.-S. (2011). A mechanism denial study on the Madden-Julian Oscillation. *Journal of Advances in Modeling Earth Systems*, *3*, n/a-n/a. https://doi.org/10.1029/2011MS000081
Kim, H., Vitart, F., & Waliser, D. E. (2018). Prediction of the Madden–Julian Oscillation: A Review. *Journal of Climate*, *31*, 9425–9443. https://doi.org/10.1175/JCLI-D-18-0210.1
Kim, H.-M., Webster, P. J., Toma, V. E., & Kim, D. (2014). Predictability and prediction skill of the MJO in two operational forecasting systems. *Journal of Climate*, *27*, 5364–5378. https://doi.org/10.1175/JCLI-D-13-00480.1
Kiranmayi, L., & Maloney, E. D. (2011). Intraseasonal moist static energy budget in reanalysis data. *Journal of Geophysical Research: Atmospheres*, *116*, D21117. https://doi.org/10.1029/2011JD016031
Lau, W. K.-M., & Waliser, D. E. (2012). *Intraseasonal variability in the atmosphere-ocean climate system* (2nd ed., p. 613). Heidelberg, Germany: Springer.
Lee, J.-E., Lintner, B. R., Neelin, J. D., Jiang, X., Gentine, P., Boyce, C. K., et al. (2012). Reduction of tropical land region precipitation variability via transpiration. *Geophysical Research Letters*, *39*, n/a-n/a. https://doi.org/10.1029/2012GL053417
Lim, Y., Son, S.-W., & Kim, D. (2018). MJO prediction skill of the subseasonal-to-seasonal prediction models. *Journal of Climate*, *31*, 4075–4094. https://doi.org/10.1175/JCLI-D-17-0545.1
Ling, J., Zhang, C., Joyce, R., Xie, P.-p., & Chen, G. (2019). Possible role of the diurnal cycle in land convection in the barrier effect on the MJO by the Maritime Continent. *Geophysical Research Letters*, *46*, 3001–3011. https://doi.org/10.1029/2019gl081962
Love, B. S., Matthews, A. J., & Lister, G. M. S. (2011). The diurnal cycle of precipitation over the Maritime Continent in a high-resolution atmospheric model. *Quarterly Journal of the Royal Meteorological Society*, *137*, 934–947. https://doi.org/10.1002/qj.809
Madden, R. A., & Julian, P. R. (1971). Detection of a 40-50 day oscillat
ion in zonal wind in tropical Pacific. *Journal of the Atmospheric Sciences*, *28*, 702.
Majda, A. J., & Yang, Q. (2016). A multiscale model for the intraseasonal impact of the diurnal cycle over the Maritime Continent on the Madden-Julian Oscillation. *Journal of the Atmospheric Sciences*, *73*, 579–604. https://doi.org/10.1175/JAS-D-15-0158.1
Maloney, E. D. (2009). The moist static energy budget of a composite tropical intraseasonal oscillation in a climate model. *Journal of Climate*, *22*, 711–729.
Maloney, E. D., & Sobel, A. H. (2004). Surface fluxes and ocean coupling in the tropical intraseasonal oscillation. *Journal of Climate*, *17*, 4368–4386.
Maloney, E. D., Sobel, A. H., & Hannah, W. M. (2010). Intraseasonal variability in an aquaplanet general circulation model. *Journal of Advances in Modeling Earth Systems*, *2*. https://doi.org/10.3894/james.2010.2.5
Mapes, B., Tulich, S., Lin, J., & Zuidema, P. (2006). The mesoscale convection life cycle: Building block or prototype for large-scale tropical waves? *Dynamics of Atmospheres and Oceans*, *42*, 3–29. https://doi.org/10.1016/J.Dynatmoce.2006.03.003
Mapes, B. E., & Bacmeister, J. T. (2012). Diagnosis of tropical biases and the MJO from patterns in the MERRA analysis tendency fields. *Journal of Climate*, *25*, 6202–6214. https://doi.org/10.1175/jcli-d-11-00424.1
Moncrieff, M. W. (2013). The multiscale organization of moist convection and the intersection of weather and climate. In *Climate Dynamics: Why Does Climate Vary?* (pp. 3-26). Boston, MA: American Geophysical Union.
Mori, S., Jun-Ichi, H., Tauhid, Y. I., Yamanaka, M. D., Okamoto, N., Murata, F., et al. (2004). Diurnal land-sea rainfall peak migration over Sumatera Island, Indonesian Maritime Continent, observed by TRMM satellite and intensive rawinsonde soundings. *Monthly Weather Review*, *132*, 2021–2039. https://doi.org/10.1175/1520-0493(2004)132<2021:DLRPMO>2.0.CO;2
Nakazawa, T. (1988). Tropical super clusters within intraseasonal variations over the western Pacific. *Journal of the Meteorological Society of Japan*, *66*, 823–839.
Neale, R., & Slingo, J. (2003). The Maritime Continent and its role in the global climate: A GCM study. *Journal of Climate*, *16*, 834–848. https://doi.org/10.1175/1520-0442(2003)016<0834:TMCAIR>2.0.CO;2
Neena, J. M., Lee, J. Y., Waliser, D., Wang, B., & Jiang, X. (2014). Predictability of the Madden-Julian Oscillation in the Intraseasonal Variability Hindcast Experiment (ISVHE). *Journal of Climate*, *27*, 4531–4543. https://doi.org/10.1175/JCLI-D-13-00624.1
Nesbitt, S. W., & Zipser, E. J. (2003). The diurnal cycle of rainfall and convective intensity according to three years of TRMM measurements. *Journal of Climate*, *16*, 1456–1475. https://doi.org/10.1175/1520-0442(2003)016<1456:TDCORA>2.0.CO;2

Oh, J. H., Kim, K. Y., & Lim, G. H. (2012). Impact of MJO on the diurnal cycle of rainfall over the western Maritime Continent in the austral summer. *Climate Dynamics*, *38*, 1167–1180. https://doi.org/10.1007/s00382-011-1237-4

Peatman, S. C., Matthews, A. J., & Stevens, D. P. (2014). Propagation of the Madden-Julian Oscillation through the Maritime Continent and scale interaction with the diurnal cycle of precipitation. *Quarterly Journal of the Royal Meteorological Society*, *140*, 814–825. https://doi.org/10.1002/qj.2161

Peatman, S. C., Matthews, A. J., & Stevens, D. P. (2015). Propagation of the Madden-Julian Oscillation and scale interaction with the diurnal cycle in a high-resolution GCM. *Climate Dynamics*, *45*, 2901–2918. https://doi.org/10.1007/s00382-015-2513-5

Qian, J.-H. (2008). Why precipitation is mostly concentrated over islands in the Maritime Continent. *Journal of the Atmospheric Sciences*, *65*, 1428–1441. https://doi.org/10.1175/2007JAS2422.1

Ramage, C. S. (1968). Role of a tropical "Maritime Continent" in the atmospheric circulation. *Monthly Weather Review*, *96*, 365–370. https://doi.org/10.1175/1520-0493(1968)096<0365:ROATMC>2.0.CO;2

Rauniyar, S. P., & Walsh, K. J. E. (2011). Scale interaction of the diurnal cycle of rainfall over the Maritime Continent and Australia: Influence of the MJO. *Journal of Climate*, *24*, 325–348. https://doi.org/10.1175/2010JCLI3673.1

Raymond, D. J., & Fuchs, Ž. (2009). Moisture modes and the Madden-Julian Oscillation. *Journal of Climate*, *22*, 3031–3046. https://doi.org/10.1175/2008jcli2739.1

Raymond, D. J., Sessions, S., Sobel, A., & Fuchs, Z. (2009). The mechanics of gross moist stability. *Journal of Advances in Modeling Earth Systems*, *1*, 20. https://doi.org/10.3894/james.2009.1.9

Salby, M. L., & Hendon, H. H. (1994). Intraseasonal behavior of clouds, temperature, and motion in the Tropics. *Journal of the Atmospheric Sciences*, *51*, 2207–2224.

Seo, K. H., & Kim, K. Y. (2003). Propagation and initiation mechanisms of the Madden-Julian Oscillation. *Journal of Geophysical Research*, *108*. https://doi.org/10.1029/2002jd002876

Slingo, J., Inness, P., Neale, R., Woolnough, S., & Yang, G. Y. (2003). Scale interactions on diurnal to seasonal timescales and their relevance to model systematic errors. *Annals of Geophysics*, *46*, 139–155.

Sobel, A., & Maloney, E. (2012). An idealized semi-empirical framework for modeling the Madden-Julian Oscillation. *Journal of the Atmospheric Sciences*, *69*, 1691–1705. https://doi.org/10.1175/jas-d-11-0118.1

Sobel, A., & Maloney, E. (2013). Moisture modes and the eastward propagation of the MJO. *Journal of the Atmospheric Sciences*, *70*, 187–192 . https://doi.org/10.1175/Jas-D-12-0189.1

Sobel, A. H., Maloney, E. D., Bellon, G., & Frierson, D. M. (2008). The role of surface heat fluxes in tropical intraseasonal oscillations. *Nature Geoscience*, *1*, 653–657. https://doi.org/10.1038/Ngeo312

Sobel, A. H., Maloney, E. D., Bellon, G., & Frierson, D. M. (2010). Surface fluxes and tropical intraseasonal variability: A reassessment. *Journal of Advances in Modeling Earth Systems*, *2*, 2. https://doi.org/10.3894/JAMES.2010.2.2

Takayabu, Y. N. (1994). Large-scale cloud disturbances associated with equatorial waves.1. Spectral Features of the Cloud Disturbances. *Journal of the Meteorological Society of Japan*, *72*, 433–449.

Tian, B., Waliser, D. E., Fetzer, E. J., & Yung, Y. L. (2010). Vertical moist thermodynamic structure of the Madden-Julian Oscillation in atmospheric infrared sounder retrievals: An update and a comparison to ECMWF Interim re-analysis. *Monthly Weather Review*, *138*, 4576–4582. https://doi.org/10.1175/2010MWR3486.1

Tian, B. J., Waliser, D. E., & Fetzer, E. J. (2006). Modulation of the diurnal cycle of tropical deep convective clouds by the MJO. *Geophysical Research Letters*, *33*. https://doi.org/10.1029/2006gl027752

TRMM (2011). Tropical Rainfall Measuring Mission (TMPA) Rainfall Estimate L3 3 hour 0.25 degree x 0.25 degree V7, Greenbelt, MD, Goddard Earth Sciences Data and Information Services Center (GES DISC). Data was downloaded from https://disc.gsfc.nasa.gov/datasets/TRMM_3B42_7/summary. Accessed: 02/15/2018, https://doi.org/10.5067/TRMM/TMPA/3H/7

Vintzileos, A., & Pan, H.-L. (2008). On the importance of horizontal resolution and initial conditions to forecasting tropical intra-seaonal oscillations: The Maritime Continent prediction barrier. http://www.nws.noaa.gov/ost/climate/STIP/CTB-COLA/Augustin_091907.htm

Vitart, F. (2017). Madden-Julian Oscillation prediction and teleconnections in the S2S database. *Quarterly Journal of the Royal Meteorological Society*, *143*, 2210–2220. https://doi.org/10.1002/qj.3079

Vitart, F., & Molteni, F. (2010). Simulation of the Madden-Julian Oscillation and its teleconnections in the ECMWF forecast system. *Quarterly Journal of the Royal Meteorological Society*, *136*, 842–855. https://doi.org/10.1002/Qj.623

Vitart, F., Robertson, A., Kumar, A., Hendon, H., Takaya, Y., Lin, H., et al. (2012). Subseasonal to seasonal prediction: Research implementation plan, WWRP/THORPEX-WCRP Report.

Wang, W., Hung, M.-P., Weaver, S., Kumar, A., & Fu, X. (2013). MJO prediction in the NCEP Climate Forecast System version 2. *Climate Dynamics*, 1–12. https://doi.org/10.1007/s00382-013-1806-9

Weaver, S. J., Wang, W., Chen, M., & Kumar, A. (2011). Representation of MJO variability in the NCEP Climate Forecast System. *Journal of Climate*, *24*, 4676–4694. https://doi.org/10.1175/2011JCLI4188.1

Wheeler, M. C., & Hendon, H. H. (2004). An all-season real-time multivariate MJO index: Development of an index for monitoring and prediction. *Monthly Weather Review*, *132*, 1917–1932.

Wolding, B. O., Maloney, E. D., & Branson, M. (2016). Vertically resolved weak temperature gradient analysis of the Madden-Julian Oscillation in SP-CESM. *Journal of Advances in Modeling Earth Systems*. https://doi.org/10.1002/2016MS000724

Wu, C.-H., & Hsu, H.-H. (2009). Topographic Influence on the MJO in the Maritime Continent. *Journal of Climate*, *22*, 5433–5448. https://doi.org/10.1175/2009JCLI2825.1

Xiang, B., Zhao, M., Jiang, X., Lin, S.-J., Li, T., Fu, X., & Vecchi, G. (2015). 3-4 week MJO prediction skill in a GFDL Coupled Model. *Journal of Climate*. https://doi.org/10.1175/JCLI-D-15-0102.1

Yanai, M., Esbensen, S., & Chu, J.-H. (1973). Determination of bulk properties of tropical cloud clusters from large-scale heat and moisture budgets. *Journal of the Atmospheric Sciences*, *30*, 611–627.

Yanai, M., & Johnson, R. H. (1993). Impacts of cumulus convection on thermodynamic fields. In K. A. Emanuel & D. J. Raymond (Eds.), *The Representation of Cumulus Convection in Numerical Models* (pp. 39–62). Boston, MA: American Meteorological Society.

Yang, G. Y., & Slingo, J. (2001b). The diurnal cycle in the Tropics. *Monthly Weather Review*, *129*, 784–801.

Zhang, C. (2013). Madden-Julian Oscillation: Bridging weather and climate. *Bulletin of the American Meteorological Society*, *94*, 1849–1870. https://doi.org/10.1175/bams-d-12-00026.1

Zhang, C., & Hendon, H. H. (1997). Propagating and standing components of the intraseasonal oscillation in tropical convection. *Journal of the Atmospheric Sciences*, *54*, 741-752. https://doi.org/10.1175/1520-0469(1997)054<0741:PASCOT>2.0.CO;2

Zhang, C., & Ling, J. (2017). Barrier effect of the Indo-Pacific Maritime Continent on the MJO: Perspectives from tracking MJO precipitation. *Journal of Climate*, *30*, 3439-3459. https://doi.org/10.1175/JCLI-D-16-0614.1

Zhang, C. D. (2005). Madden-Julian Oscillation, *Reviews of Geophysics*., *43*, RG2003. https://doi.org/10.1029/2004RG000158